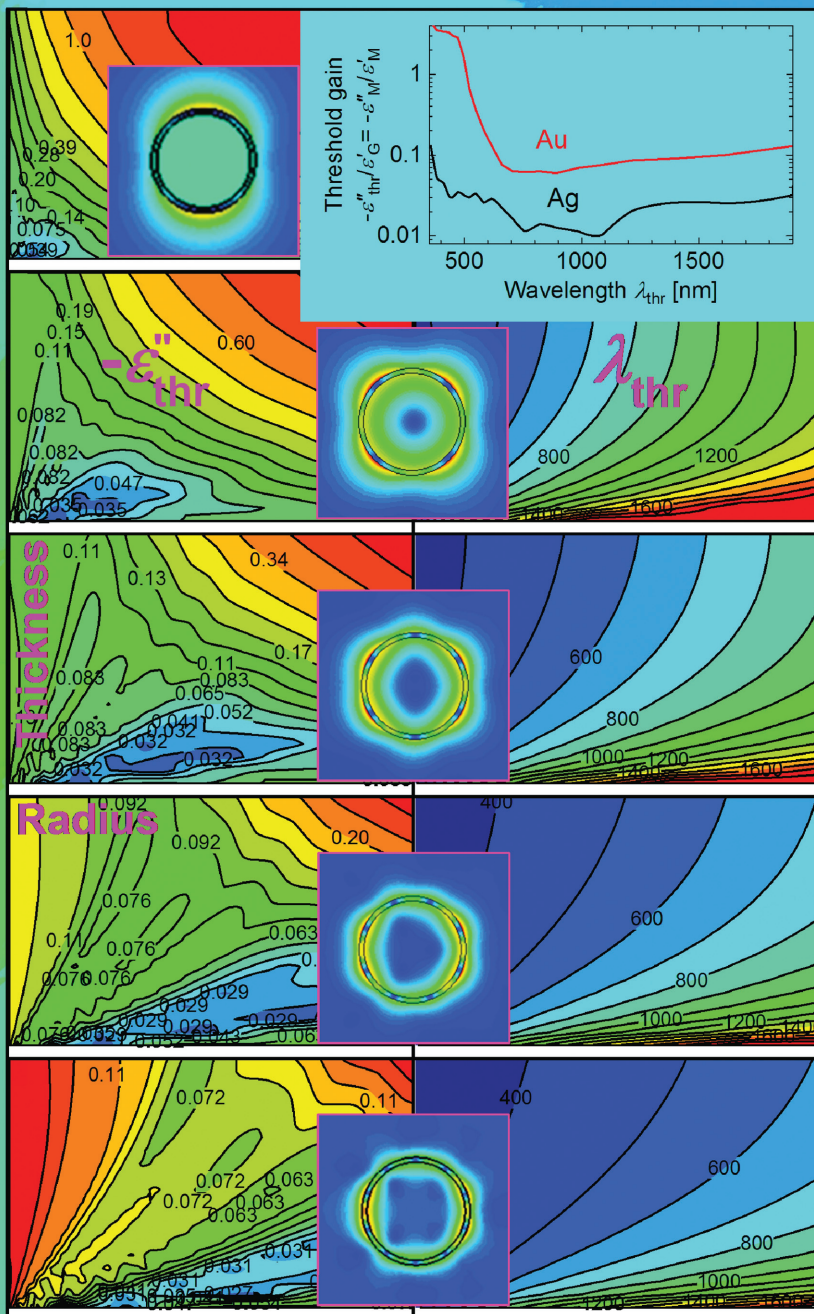# annalen der physik

Minimal spaser threshold within electrodynamic framework: Shape, size and modes

by Nikita Arnold, Calin Hrelescu and Thomas A. Klar

WILEY-VCH

Minimal spaser threshold within electrodynamic framework: Shape, size and modes

Nikita Arnold[1,2,*], Calin Hrelescu[1], and Thomas A. Klar[1]

It is known (yet often ignored) from quantum mechanical or energetic considerations, that the threshold gain of the quasi-static spaser depends only on the dielectric functions of the metal and the gain material. Here, we derive this result from the purely classical electromagnetic scattering framework. This is of great importance, because electrodynamic modelling is far simpler than quantum mechanical one. The influence of the material dispersion and spaser geometry are clearly separated; the latter influences the threshold gain only indirectly, defining the resonant wavelength. We show that the threshold gain has a minimum as a function of wavelength. A variation of nanoparticle shape, composition, or spasing mode may shift the plasmonic resonance to this optimal wavelength, but it cannot overcome the material-imposed minimal gain. Furthermore, retardation is included straightforwardly into our framework; and the global spectral gain minimum persists beyond the quasi-static limit. We illustrate this with two examples of widely used geometries: Silver spheroids and spherical shells embedded in and filled with gain materials.

1 Introduction

Over the last decade, many groups investigated plasmonic devices coupled to gain materials both theoretically and experimentally. The promise of plasmonics is to defy the diffraction limit using evanescence and local field enhancement inherent for plasmonic nanostructures. However, those strategies are hampered by significant Joule losses of the metals in the visible (VIS) and near infrared (IR) range of the optical spectrum. The combination of metals with active (gain) materials may compensate these losses [1, 2], narrow the resonances [3] and ultimately lead to amplification and generation of evanescent modes [4, 5]. This, for instance, increases the sensitivity in sensing applications [6]. Besides, the integration of plasmonic devices on a chip requires active elements, such as emitters, amplifiers and generators. A related field of studies is loss compensation in metamaterials, which prevents absorption losses from degrading all the important figures of merit [7–17].

A spaser fully nanoscopic in all three dimensions was first suggested by Bergman and Stockman [4]. Similar concepts were discussed by others [3, 18]. Experimental confirmation of such a spasing has been claimed recently for metal nanoparticles using pulsed optical pumping and high thresholds. Indeed, we show in this contribution, that the spectral position of plasmonic resonances used in [19, 20] is sub-optimal and requires very high gain. Related research areas are "plasmonic nanolasers", where, however, at least one dimension is not truly nanoscopic [21–31], and the amplification and generation of surface plasmon polaritons [1, 32–35].

A detailed theoretical analysis of spaser operation can be found for example in [5, 36–40], and numerical time domain analyses of active media with applications to metamaterials were recently performed in [15, 41]. These works either describe both the plasmonic electromagnetic (EM) field and the gain medium (*e.g.,* chromophores or semiconductor nanocrystals) by quantum mechanics, or use rate equations for the populations of the chromophores' energy levels, while treating the polarization and the resulting EM-fields semi-classically. While such "first principles" approaches provide most

* Corresponding authors E-mail: nikita.arnold@jku.at
1 Institute of Applied Physics, Johannes Kepler University Linz, Altenbergerstraße 69, 4040 Linz, Austria
2 Soft Matter Physics, Johannes Kepler University Linz, Altenberger-straße 69, 4040 Linz, Austria

detailed analyses, they are in many cases of limited transparency. In contrast, purely classical electrodynamics is far easier to interpret and, most important, gives useful predictions as long as the spasing threshold is approached from below, increasing the gain level towards the threshold value [5]. Specifically, the threshold gain itself can be determined using classical physics. Hence, we will apply electrodynamic analysis utilizing a negative imaginary part of the dielectric function (or absorption coefficient) in this work.

In typical experimental situations, one deals not with a single or a few active chromophores or quantum dots, but with hundreds or thousands of them. Hence, the concentration of active molecules, rather than their individual quantum-mechanical properties usually limits the feasibility of the spaser. This also favors a macroscopic approach, which was used in calculations performed recently [19, 20, 42–55]. In these papers, the influence of the nanostructures' geometry on the spasing modes and the generation thresholds was studied with different degrees of detail. Earlier considerations on these topics are given in the papers [3, 56, 57]. Further, the interaction of metal nano-particles with a single or multiple active Hertzian dipole emitters was investigated in a series of numerical studies [58–60].

In the current paper, we show that many previous calculations, aiming to decrease the spasing threshold by applying different shapes, aspect ratios or even multipolar modes of spasers, can be boiled down to a very general spasing threshold, which depends only on the materials constants as long as the spaser is small enough to be in the electrostatic limit. For somewhat larger particles, as long as one remains in the near–field framework, the threshold can only increase due to scattering losses. (We note in passing, that geometric resonances appear for structure sizes comparable with the wavelength in the gain material [61], and the thresholds can become arbitrarily low [47].) As the materials parameters show dispersion, the lasing threshold shows a dispersion, too, with several local minima for specific wavelength ranges and a global minimum in the deep red to near IR for Au and Ag spasers, respectively. Changes in shape, aspect ratios or spasing modes may only be used to shift the spasing eigenfrequency towards those minima, but not to change them in any way. Although similar results have been derived before for the specific example of spheroids [56], by using general energy considerations [62], or by using quantum mechanics [63], it seems that they have been widely overlooked given the large body of publications named previously, where one tried to improve spaser thresholds using specific nanoparticle geometries, and modes.

We give explicit minimal values for the threshold gain for gold and silver spasers based on experimental dielectric constants. We find that the minimal gain necessary for spasing is below $6 \cdot 10^2$ cm^{-1} for silver and $5 \cdot 10^3$ cm^{-1} for gold, both in the red to near IR wavelengths. To show how the retardation increases the necessary gain via scattering losses, we analytically consider two experimentally important examples of nanorods and core-shell systems. In the VIS, the scattering losses quickly increase the required gain to levels hardly achievable with currently available materials. The situation is better in the IR. For the core-shells, we find that for higher order modes the influence of scattering losses settles in at larger structure sizes and is less severe.

2 A simple example

Let us first consider an illustrative example, which we subsequently generalize. The dipolar polarizability of a small metallic rotational ellipsoid (volume V, depolarization factor L (see Supp. Info. 1), dielectric constant ε_M) embedded in a gain material (dielectric constant ε_G) is in CGS units [64]:

$$\alpha = \frac{(V/4\pi)(\varepsilon_M - \varepsilon_G)}{L\varepsilon_M + (1-L)\varepsilon_G} \tag{1}$$

The denominator, which we hence denote as D, is a complex-valued function of frequency ω (or wavelength λ) due to the dispersion of the dielectric functions. In case of spherical particles, $L = 1/3$, which leads to the characteristic Clausius-Mossotti denominator:

$$3D = \varepsilon_M + 2\varepsilon_G = \varepsilon_M'(\lambda) + 2\varepsilon_G'(\lambda) + i(\varepsilon_M''(\lambda) + 2\varepsilon_G''(\lambda)) \tag{2}$$

A minimum of $|D|$ corresponds to a peak in polarizability, as well as in scattering and absorption cross sections [65]. For a transparent host medium with $\varepsilon_G'' = 0$, the condition $\varepsilon_M'(\lambda) + 2\varepsilon_G'(\lambda) = 0$ defines the position of the dipolar resonance, while $\varepsilon_M'' > 0$ limits its strength and width [62, 64]. If an optical gain $-\varepsilon_G'' > 0$ is present, it compensates Ohmic losses in the metal. With $\varepsilon_G' = -\varepsilon_M'/2$ and simultaneously $\varepsilon_G'' = -\varepsilon_M''/2$, the denominator D in (2) vanishes, which leads to singularities in the polarizability and in the cross-sections. This corresponds to a spasing threshold, because a singular polarizability can amplify an infinitely small spontaneous emission noise to a finite field value. From the mathematical viewpoint $D = 0$ allows solution with non-zero polarization without an external field. Roughly speaking, the imaginary part in (2) defines the threshold gain, while the real part defines the generation wavelength. Note, that post-threshold

Ann. Phys. (Berlin) **528**, No. 3–4 (2016)

annalen
der **physik**

Original Paper

operation of a spaser, as well as threshold fields, are determined by non-linear gain saturation [5, 51, 66]. In particular, very high fields and/or cross-sections obtained in linear studies [43, 48, 50, 54, 55, 67, 68] are unphysical. However in this paper, we are interested only in threshold gain and wavelength, which, as for the conventional lasers, can be deduced from a linear theory [69, 70].

In the visible, $0.2 < \varepsilon''_{Ag} < 0.3$ for silver, while for gold ε''_{Au} is one order of magnitude larger [71]. Thus, the gain threshold can be estimated to be $\varepsilon''_G \sim -\varepsilon''_M/2 \sim -0.1$ for spherical Ag nanoparticles in the VIS. These values can be related to the experimentally more accessible amplification β:

$$\beta = c_{dye}\sigma_{dye} = -2kn''_G \sim 10^3 \text{cm}^{-1} \tag{3}$$

Here $k = 2\pi/\lambda$ is the vacuum wavenumber and $n_G = \sqrt{\varepsilon_G}$ is the refractive index of a (non-magnetic) gain medium. The typical value of $\beta = 10^3 \text{cm}^{-1}$ was obtained assuming an emission cross-section of the dye molecules of $\sigma_{dye} \sim 10^{-16}\text{cm}^2$, and a population inversion concentration of $c_{dye} \sim 10^{19}\text{cm}^{-3}$. This can be recalculated into ε''_G by

$$\varepsilon''_G = 2n'_G n''_G \approx -n_{host}\beta\lambda/2\pi$$
$$= -n_{host}c_{dye}\sigma_{dye}\lambda/2\pi \sim -0.0102 \tag{4}$$

Here we assumed a representative value $\lambda = 400$ nm and $n_{host} = 1.6$. This value is almost one order of magnitude lower than what is required for the dipole-mode threshold in Ag spheres, which is the weakest absorber in the VIS among the noble metals. Some chromophores have $\sigma_{dye} \sim 4 \cdot 10^{-16}\text{cm}^2$ and concentrations may be increased up to $c_{dye} \sim 2.5 \cdot 10^{19}\text{cm}^{-3}$ without aggregation, which would result in $\varepsilon''_G \approx -0.1$. However, in practice, chromophores tend to photo-bleach and degrade with time, plasmon damping is increased in nano-structures due to electron collisions with the boundaries [64], and part of the chromophores' excitations decay spontaneously into plasmon-polaritons in the vicinity of metal features, etc. All these parasitic effects increase the threshold gain requirements further, but are beyond the scope of this article where we aim to find lower bounds for the spasing gain threshold.

3 Minimal threshold for the quasi-static limit

The denominator of equation (1) (up to a constant factor) can be rewritten in the form

$$D = \varepsilon_G + N\varepsilon_M \tag{5}$$

with

$$N = L/(1 - L) \tag{6}$$

in case of the dipolar resonance of rotational ellipsoids, as was used by Smuk and Lawandy [56]. In the current paper, however, we argue that in the quasi-static limit the resonant denominator may be rewritten in the form of equation (5) for *any* shape and *any* multipolar order. For example, the l-th multipolar mode of a small (non retarded) metallic sphere immersed in a gain medium shows a resonant denominator (5) with (see Supp. Info. 2)

$$N = l/(1 + l) \tag{7}$$

while in the opposite case, a gain containing void inside a metal requires (Supp. Info. 2)

$$N = (1 + l)/l \tag{8}$$

Further down, we will discuss the case of a metallic shell of thickness h, whereby the gain material is distributed inside the core of the shell (radius a) and also outside. The small-particle and thin shell limit leads to (Eqn. (S.30) in Supp. Info. 6):

$$N = \frac{l(l+1)}{2l+1}\frac{h}{a} \tag{9}$$

For the quasi-static shell of arbitrary thickness, expressions (S.28) can be used. Even with particle dimers, the shape parameter N depends only on geometry. As illustrated in Supp. Info. 7, we derive for the "bright, in-phase" quasi-static dipolar mode of two equal prolate spheroids aligned along long semi-axis c (short semi-axes a) with center separation R:

$$N = \frac{L - v}{1 - L + v}, \quad \text{with} \quad v = \frac{2a^2c}{3R^3} \tag{10}$$

In all these cases, N and hence the denominator (5) is a function of the multipolar order l and the geometry (given, for instance, by the depolarization factor L or by the relative thickness of the metallic shell h/a).

The requirement $D = 0$, and the separation of the real and imaginary parts in the Eqn. (5) yields $\varepsilon'_G = -N\varepsilon'_M$ and $\varepsilon''_G = -N\varepsilon''_M$, which can be rewritten into:

$$N(\text{geometry, mode}) = -\frac{\varepsilon'_G}{\varepsilon'_M} \quad \text{and} \quad \varepsilon''_G = \frac{\varepsilon''_M}{\varepsilon'_M}\varepsilon'_G \tag{11}$$

Note, that typically, $\varepsilon'_G > 0$, $\varepsilon'_M < 0$, $\varepsilon''_G < 0$, $\varepsilon''_M > 0$, and $N > 0$. The geometry of the nano-particle, and the mode used for spasing, influence only the shape-mode

parameter N. It can be derived analytically (examples are given by the equations (6)-(10)), numerically, or estimated experimentally, using the 1st of Eqns. (11) and the spectral position of the resonant wavelength. If N is known, the 1st equality in (11) defines a wavelength λ_{thr} due to the dispersion of dielectric functions ε'_M and ε'_G, while the 2nd one determines the threshold gain $-\varepsilon''_G > 0$ at this wavelength. Alternatively, the 1st equation in (11) can be used to find N, which can provide the resonance at a given wavelength. Relevant N values range from 10^{-2} to 1, and can be obtained by *continuously* varying the geometry of an *arbitrary* nanoparticle: for example the aspect ratio of rods according to eq. (6), or relative shell thickness via equation (9), or changing the multipolar order l. If the shape of the metal nanoparticle (and therefore, N) is fixed, the resonance can still be shifted to the desired wavelength, choosing the host material for the active molecules with the appropriate ε'_G.

Different particle geometries and/or mode numbers l may result in the same N values, as can be seen for instance from the Eq. (9), and will be further illustrated below. Structures with the same N have the same resonant wavelength and threshold gain values. The 2nd equality in (11), defining the threshold gain, is independent from any geometrical parameter or multipole order, and depends only on the dispersion of the materials at the resonant wavelength. The latter, of course, depends on the geometry via the shape-mode factor N. The *minimal possible* threshold gain can be found by minimizing the 2nd expression (11) as a function of wavelength, irrespectively of particle shape. Any nanoparticle shape, or spasing mode, that has the value of N resulting in resonance at the wavelength of minimal gain is equally effective.

Figure 1a shows the dependences $N(\lambda)$ (dashed) and $-\varepsilon''_G(\lambda)$ (solid) defined by the relations (11) for silver and gold with dielectric functions from Johnson and Christy [71] and normalized to the real part ε'_G of the gain material. For $\varepsilon'_G \neq 1$ the results simply rescale, with larger ε'_G resulting in larger threshold gain and N values, a fact that should be considered in the selection of a suitable gain medium. The global minima around 1060 nm for silver and around 750 nm for gold can be understood in the following way: To reduce the required gain, N should be decreased, because of $-\varepsilon''_G = N\varepsilon''_M$. The decrease in N by shape-tuning, *e.g.*, increase in the aspect ratio of nanorods (eq. (6)), or by using thinner shells (eq. (9)), unavoidably red-shifts the plasmon resonance because of $-\varepsilon'_G = N\varepsilon'_M$. However, for metals ε''_M increases with wavelength. This counteracts the decrease in N and leads to a global minimum. To elaborate on these trends, Supp. Info. 3 provides formu-
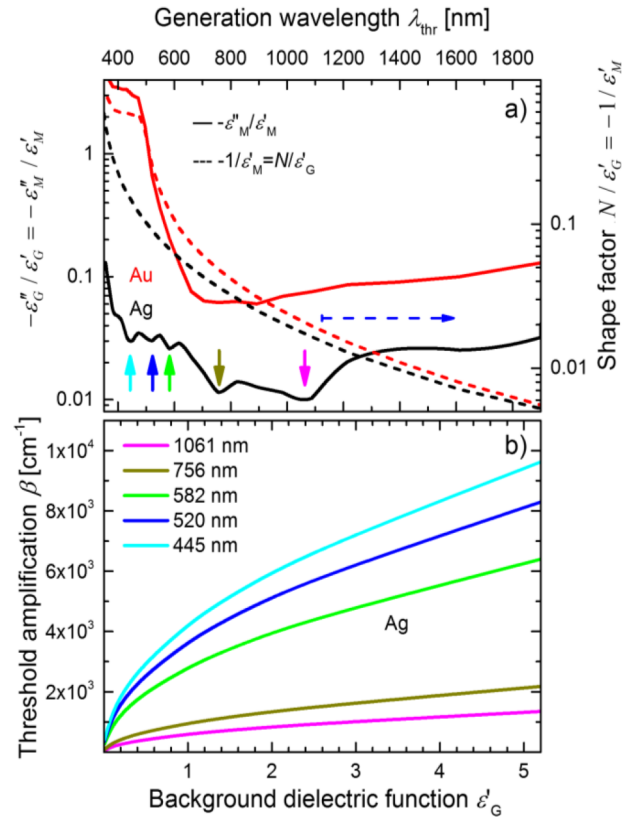

Figure 1 Universal quasi-static threshold parameters. a) Solid curves (left scale) show the dependence of $-\varepsilon''_M/\varepsilon'_M$ on the wavelength λ for Ag (black) and Au (red) with Johnson and Christy values. The threshold gain $-\varepsilon''_G$ can be obtained from this ratio by multiplying it with ε'_G of the gain material. Dashed curves (right scale) show the corresponding $-1/\varepsilon'_M$ values, which are equal to the normalized shape factor N/ε'_G at the threshold. Both ordinates have logarithmic scales. b) Dependences of the threshold amplification β on the background dielectric ε'_G for 5 local minima of the $-[\varepsilon''_M/\varepsilon'_M](\lambda)$ curves for Ag, as color-coded in the legend.

las for a general Drude metal. The full red line in Fig. 1a predicts for example, that small Au spheres, or short rods with the resonances in the range $500 < \lambda < 600$ nm used in Refs.19, 20, are expected to have thresholds that exceed the optimal values by a factor of 6–10, and that of Ag by a factor of 20–50. In Fig. 1b we plot the dependence of the amplification β for the five local minima of gain that can be seen in the black solid curve for Ag in Fig. 1a. Note that data in Fig. 1 use bulk values for gold and silver, neglecting surface induced damping. Hence, if the wavelength of minimal necessary gain (defined by the right expression in (11)) can be reached with several different geometries (which all may fulfill the left equality in (11)), the one with the smallest surface to volume ratio should be used to minimize losses by surface damping.

Ann. Phys. (Berlin) **528**, No. 3–4 (2016)

annalen
der **physik**

Original Paper

Table 1 Minimally required amplification in cm^{-1} and required imaginary part of the gain dielectric constant $-\varepsilon_G'' = -\varepsilon_{thr}''$ to reach spasing threshold, assuming $\varepsilon_G' = 1$

	500 nm		750 nm		1060 nm		1500 nm	
	β [cm^{-1}]	$-\varepsilon_{thr}''$	β [cm^{-1}]	$-\varepsilon_{thr}''$	β [cm^{-1}]	$-\varepsilon_{thr}''$	β [cm^{-1}]	$-\varepsilon_{thr}''$
Ag	$4.0\cdot10^3$	0.032	$9.9\cdot10^2$	0.012	$5.9\cdot10^2$	0.010	$1.1\cdot10^3$	0.026
Au	$1.6\cdot10^5$	1.5	$5.2\cdot10^3$	0.062	$4.3\cdot10^3$	0.073	$4.0\cdot10^3$	0.095

We give the absolute numbers for the threshold gain $-\varepsilon_G''$ and amplification β for four typical wavelength ranges in 1 Around 500 nm, where small spherical gold nanoparticles show their plasmon resonance, around 750 nm and 1060 nm where the minimally required gain is achieved for Au and Ag, and around 1500 nm, which is important for telecom applications. The feasibility of such a gain under injection or continuous optical pumping was put in doubt in [72, 73]. However, in the pulsed regime the concomitant thermal problems look tolerable. Indeed, with sub-ps optical pumping, the threshold population inversion $c_{dye} \sim 10^{19}$cm^{-3} can be reached almost without losses. Even if a significant fraction of the electronic excitation is converted into heat during the generation stage, the associated temperature rise ΔT can be estimated from the energy balance per unit volume of the gain material: $C_p\rho\Delta T \sim c_{dye}\hbar\omega < 10$ J cm^{-3}, which for a typical volumetric heat capacity $C_p\rho \sim 1$ J cm^{-3}K^{-1} results in $\Delta T < 10$ K.

Although we arrived at our conclusions using illustrative examples, equation (11) holds for *any* geometry or multipolar order, as it represents the lowest term in the Taylor expansion of the *arbitrary* resonant scattering denominator with respect to particle size (see Section 6). A similar expression was derived from general energetic considerations by Wang and Shen [62], who, however, did not discuss the consequences for spaser optimization. One can also show that our condition (11) coincides with equation (82) and Fig. 26 of the paper by Stockman [63] in the case of weak relaxation $\varepsilon_M'' << -\varepsilon_M'$. Local spectral minima in Figs. 26 and 1a (solid curves) are the same, because ε_M data from [71] were used in both cases. The representative β values from Table 1 (g_{th} in [63]) become similar to those in Fig. 26 after rescaling with $g_{th} = \beta \propto \sqrt{\varepsilon_G'}$ (see Eqn. (4)) and (11). Alternatively, one can use the Fig. 1b for comparison. For example, the deepest minimum for Ag (magenta curve for $\lambda_{thr} \approx$ 1060 nm ↔ 1.17 eV) for $\varepsilon_d = \varepsilon_G' = 2$, results in $g_{th} = \beta \approx$ 850 cm^{-1}, in agreement with Fig. 26a. The numbers at other wavelengths are similarly consistent.

While in [63] quasistatic quantum mechanics was considered, our current argumentation relies only on macroscopic electrodynamics, does not use resonant and weak relaxation approximations and treats active chromophores, which influence ε_G'' in the optical problem, self consistently. Both approaches require small structures, but are valid for arbitrary shapes and multipolar orders, as long as retardation can be neglected. Our classical framework is easily extendable to finite sizes (see below), whereby an increase in size leads to an increase in threshold due to radiative losses. It can be shown, that threshold population inversion implied by the second expression in (11) is inversely proportional to the square of the dipole matrix element of lasing transition, in agreement with the quasi-classical results [18, 49].

While we assumed a dispersion-less ε_G in the main text, we discuss the case of a Lorentzian gain in Supp. Info. 4, taking into account its width and detuning between the plasmon and gain resonances. To show the generality of our ansatz, Supp. Info. 5 elaborates on polar dielectric crystals near a phonon-polariton line, which can also be used as $\varepsilon_M' < 0$ materials around $\lambda \approx 10$ μm instead of metals [74–76], and we find similar results.

After these general considerations for non-retarded systems, which are independent on particle shape and mode order, we discuss below two specific examples in order to illustrate the role of retardation: spheroids and nanoshells.

4 Gain thresholds for spheroidal spasers, including retardation

Spheroidal nanoparticles in gain materials were studied before in the electrostatic limit [45, 56], and experimental results for aggregates of nanoparticles were simulated with spheroids as well [77, 78]. In this section, we expand the theoretical considerations to spheroids of finite size where radiation damping and retardation are taken into account. In the non-retarded case, equations (5) and (6) hold, whereby $L = L_z$ and $L = L_{x,y}$ for the long axis in the prolate and oblate cases, respectively, are given in Supp. Info. 1. We consider only long wavelength resonances, because the short wavelength resonances overlap with the d-band absorption and are hence less suited for spasing. The results for the quasistatic, non-retarded limit are shown in Fig. 2 by black curves.

For spheroids of finite size, we use two approximations, one by Kuwata and coworkers [79] and one by Moroz [80]. Kuwata et al. suggested the following empirical formula for the resonance denominator of the
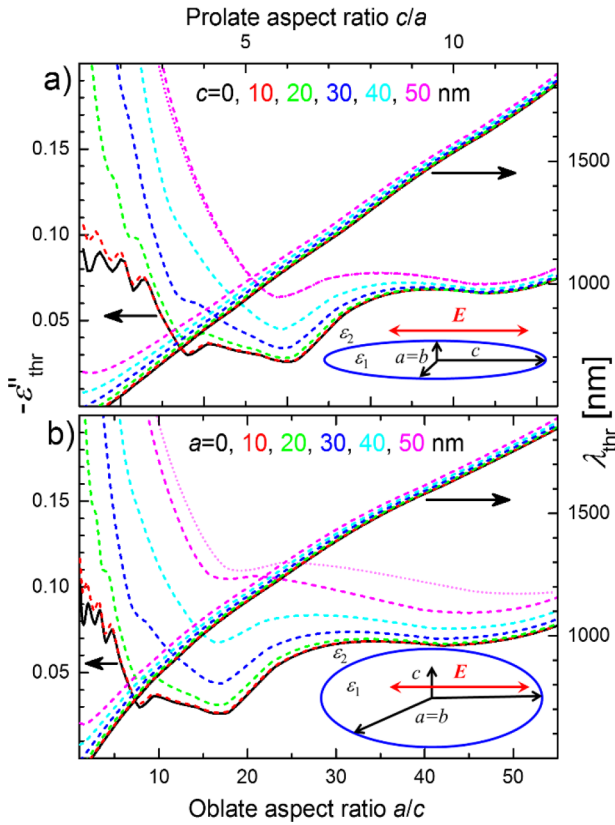
Original Paper

Figure 2 Dipolar thresholds for prolate a) and oblate b) Ag spheroids. Spheroids with $\varepsilon_1 = \varepsilon_{Ag}$ are immersed in a gain medium with $\varepsilon_2 = 2.6 + i\varepsilon_2''$. The threshold gain values: $-\varepsilon_2'' = -\varepsilon_{thr}''$ are shown at the left ordinate and the generation wavelengths at the right (as indicated by the horizontal arrows), both as functions of the aspect ratio. Insets show the structure geometry with the incident field oriented along the longer axes in both cases. Black solid curves (indexed as $c=0$ and $a=0$) correspond to the non-retarded case. Dashed curves include retardation according to Kuwata. The approximation by Moroz yields similar results as illustrated by the dotted magenta curves. The length of the largest semi-axis (c for the prolate case in a) and $a = b$ for the oblate case in b) is chosen as the size parameter and is color-coded in the plots.

dipolar polarizability:

$$D = \varepsilon_1 L + \varepsilon_2(1 - L)$$
$$+ (\varepsilon_2 - \varepsilon_1)\left(A\varepsilon_2(ka_E)^2 - B\varepsilon_2^2(ka_E)^4 + i\frac{\varepsilon_2^{3/2}k^3 V}{6\pi}\right);$$

$$A = 0.4865L + 1.046L^2 - 0.8481L^3;$$

$$B = 0.01909L + 0.1999L^2 + 0.6077L^3 \tag{12}$$

Here a_E is the semi-axis along the electric field direction and V is the volume of the spheroid, while ε_1 and ε_2 refer to the spheroid and the ambient, respectively, as shown

in the insets in Fig. 2. Moroz suggests several approximations. We choose the one implied by his equations (36), (37), (56), which empirically correct the dynamic depolarization factors Δ for the inhomogeneity of the field profile inside the particle.

$$D = \varepsilon_1 L + \varepsilon_2(1 - L)$$
$$+ (\varepsilon_2 - \varepsilon_1)\left(\frac{\varepsilon_2 k^2 V}{4\pi a_E}(0.37 + 0.63\Delta) + i\frac{\varepsilon_2^{3/2}k^3 V}{6\pi}\right);$$

$$\Delta_z = \frac{3}{4} \cdot \begin{cases} \dfrac{1 + e^2}{1 - e^2}L_z + 1 \\ (1 - 2e^2)L_z + 1 \end{cases};$$

$$\Delta_{x,y} = \frac{a}{2c} \cdot \begin{cases} \dfrac{3}{2e}\ln\dfrac{1 + e}{1 - e} - \Delta_z, & \text{prolate} \\ 3e^{-1}\sqrt{1 - e^2}\arcsin e - \Delta_z, & \text{oblate} \end{cases} \tag{13}$$

The dashed curves in Fig. 2 relate to equation (12) and give the threshold gain values (left ordinates) as a function of aspect ratio, whereby the long half axis serves as a color-coded parameter. For the longest half axes ($c = 50$ nm and $a = b = 50$ nm for the prolate and oblate cases, respectively), the results according to Moroz (eq. (13)) are given as dotted curves. The Kuwata formulas give slightly larger threshold gain for prolate spheroids (Fig. 2a), and smaller ones for the oblate case (Fig. 2b). Nevertheless, both approximations yield similar results, which confirms their applicability for the considered range of sizes. The threshold gain $-\varepsilon_{thr}''$ increases with the size due to radiative losses. This increase is more pronounced for smaller aspect ratios (more spherical particles), because they undergo larger increase in volume. The retardation corrections are minimal for the spheroids with long semi-axes of 10 nm, but become quite significant for 50 nm, where the approximations (12) and (13) start to lose their validity. In accordance with the general prediction (equation (11) and Fig. 1), local threshold minima are achieved at the same wavelengths as defined by the minima of the $-\varepsilon_{Ag}''/\varepsilon_{Ag}'$ ratio for the quasi-static case. For the considered material parameters, there exists a range of optimal aspect ratios (3.4-6.6 for the prolate and 7.1-19.8 for the oblate spheroids) with low threshold gain $0.026 < -\varepsilon_{thr}'' < 0.036$ within a spectral range of 727 nm $< \lambda_{thr} < 1137$ nm. The very lowest values are reached for the aspect ratios 6 and 16.9, at a generation wavelength $\lambda_{thr} = 1061$ nm with $-\varepsilon_{thr}'' \approx 0.026$ for the prolate and oblate spheroids, respectively, but a comparable minimum exists in the far red at $\lambda_{thr} = 756$ nm, with $-\varepsilon_{thr}'' \approx 0.03$ and at aspect ratios of 3.6 and 7.8.

Ann. Phys. (Berlin) **528**, No. 3–4 (2016)

annalen der **physik**

5 Gain thresholds for finite-sized (retarded) metallic shells with different multipolar spasing modes

The quasi-static expression (7) shows that for a solid spherical metal particle in a gain medium the dipole mode $l = 1$ is the easiest to generate, as it requires the lowest gain $\varepsilon_G'' = -\varepsilon_M''/2$, while higher multipole thresholds approach the limit $\varepsilon_G'' = -\varepsilon_M''$. For the active void (eq. (8)) the situation is reversed. The dipolar mode requires *the largest gain* $\varepsilon_G'' = -2\varepsilon_M''$, while higher multipoles approach the limit $\varepsilon_G'' = -\varepsilon_M''$. Metallic nano-shells which have gain both inside and outside (see sketch in the upper right hand corner of Fig. 3), possess both sphere- and void-like features, which makes their ordering of thresholds worth to investigate. For the most of the remaining section, we focus on the symmetric structures, with the same gain material inside and outside a silver shell of radius a_1 and thickness h_2. A comparison with asymmetric gain distributions, where the gain is either only in the core, or only outside the shell will be given at the end of this section. We will call the symmetric geometry GMG (gain/metal/gain), the case of a gain filled shell with passive dielectric ε_3 outside GMε_3, and the case of a metallic shell on a gainless core, but with gain outside a ε_1MG structure. Asymmetric structures have been discussed before [5, 57], but largely for the quasi-static dipole case and without global gain optimization via geometry. We note that in the main text, we use full analytical multi-shell Mie theory without approximations. *Quasi-static* approximations can be found in Supp. Info. 6.

We will now study the multipolar thresholds of the retarded GMG structures in detail. The shell is made of Ag, ($\varepsilon_2 = \varepsilon_{Ag}$), while the active material is characterized by a dispersionless $\varepsilon_1 = \varepsilon_3$ where ε_1'' defines the gain strength. The Fig. 3 shows the numerical solution of the complex-valued equations $D_l(\varepsilon_1'', \lambda) = 0$ where D_l is the multi-shell Mie denominator for each multipolar order l. No approximations were used, *i.e.,* the full denominators from [81] were employed. The left column presents the gain thresholds $-\varepsilon_{thr}''$, while the right column shows the corresponding generation wavelengths λ_{thr}. Both $-\varepsilon_{thr}''$ and λ_{thr} functions are plotted as two-dimensional contour plots of a_1 and h_2 for different multipolar modes from $l = 1$ (dipole) to $l = 5$. We make several observations: For quasi-static structures the threshold should depend only on the shape, *i.e.,* the aspect ratio h_2/a_1 (as illustrated by equation (9)). While this can clearly be seen for the higher order multipoles with $l > 2$ and for $h_2 < 10\,\text{nm}$ and $a_1 < 100$ to $200\,\text{nm}$, it is less obvious for $l = 1$ and $l = 2$. The reason is that significant retardation starts
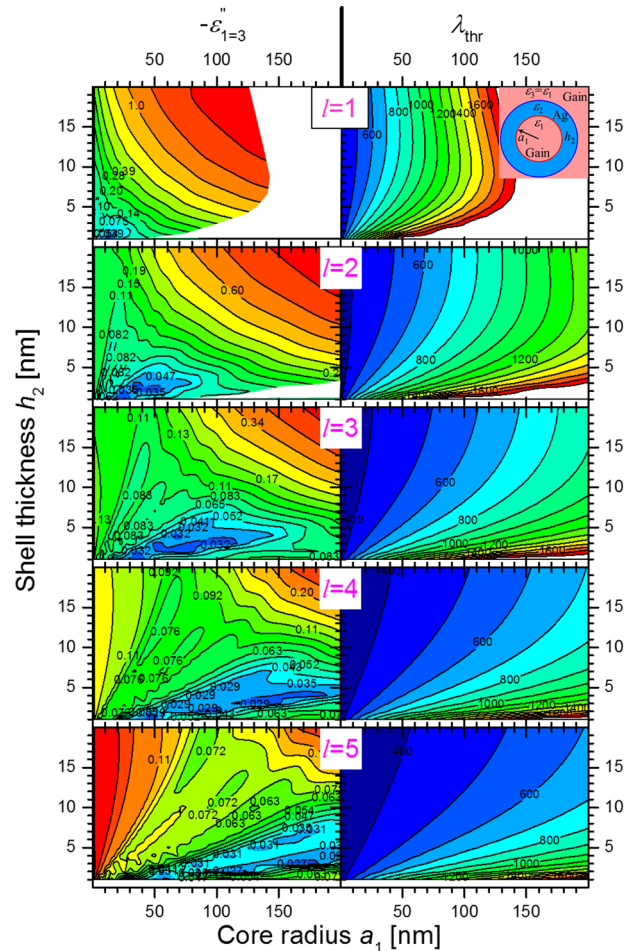

Figure 3 Multipolar thresholds for metallic shells. The inset shows the geometry of the GMG structure. A metallic shell with the dielectric function $\varepsilon_2 = \varepsilon_{Ag}$ from Johnson and Christy is immersed into and filled with a gain medium with $\varepsilon_3 = \varepsilon_1 = 2.6 + i\varepsilon_1''$. The threshold gain values $-\varepsilon_1'' = -\varepsilon_{thr}''$ (left column, log-color map) and the wavelengths λ_{thr} (right) are shown as contour plots as a function of the inner radius a_1 and the shell thickness h_2. Different plots correspond to different multipolar modes from $l = 1$ (dipole), to $l = 5$, as labeled in the panels.

very early for the low order modes: $-\varepsilon_{thr}''$ and λ_{thr} visibly deviate from the straight lines $h_2/a_1 = const$ for $a_1 \sim 10$ to $20\,\text{nm}$ and $h_2 \sim 1$ to $2\,\text{nm}$ in case of $l = 1$. The retardation settles in later for the higher multipoles, which can be seen from the corrections to Eqn. (9) (see Supp. Info. 6), which contains l in the denominator of the leading correction term. For the high order mode with $l = 5$, this occurs in the range $a_1 \sim 150$ to $200\,\text{nm}$ and $h_2 \sim 10$ to $20\,\text{nm}$. Nevertheless, the thresholds for different multipoles behave similarly. This is especially obvious for the higher multipoles. Increasing size ultimately makes

thresholds higher, similarly to the case of spheroids (Fig. 2).

The minimal possible gain is again $-\varepsilon''_{\text{thr}} = 0.026$ near $\lambda_{\text{thr}} = 1061$ nm, and $-\varepsilon''_{\text{thr}} \approx 0.03$ near $\lambda_{\text{thr}} = 756$ nm. These numbers are independent of the multipolar index l, but are achieved for different geometries, which depend on l. There exists an optimal aspect ratio h_2/a_1 for each multipolar order, for example $0.07 < h_2/a_1 < 0.15$ for the dipole and $0.015 < h_2/a_1 < 0.05$ for the $l = 5$ mode, where the threshold gain lies in the range $0.026 < -\varepsilon''_{\text{thr}} < 0.036$ (blue areas in the left column of Fig. 3).

The optimal ratio h_2/a_1 decreases with increasing multipolar index l, as expected from the approximation (9), which provides N in the universal quasi-static condition (11) for thin shells. In practical terms, the dipolar mode has low thresholds only for very small structure sizes where manufacturing is difficult and size-related effects (quantization, increased losses due to surface scattering and quenching) will hinder experimental realization. The different panels in Fig. 3 show, that it is not easy to predict a priori the mode with the lowest threshold for the given geometry. For a representative case of $a_1 = 100$ nm, $h_2 = 5$ nm the thresholds for increasing mode-order are: $-\varepsilon''_{\text{thr}} \approx 0.67$, 0.11, 0.052, 0.032, and 0.052. Thus, the mode with $l = 4$ will be "the easiest to generate" (near $\lambda_{\text{thr}} = 736$ nm), while it will be virtually impossible to "fire up" the dipolar mode.

An infinite gain medium may contain exponentially growing solutions. This is known to cause non-trivial issues in Fresnel formulas, as well as in total internal reflection (see [82] and refs. therein). However, these issues do not influence the threshold gain and wavelength, obtained from zeroes of scattering denominators, which are related to the multipolar solutions of plasmonic structures, even if the corresponding outgoing scattered waves are amplified at larger distances. To illustrate this, we compare the GMG structure studied in Fig. 3
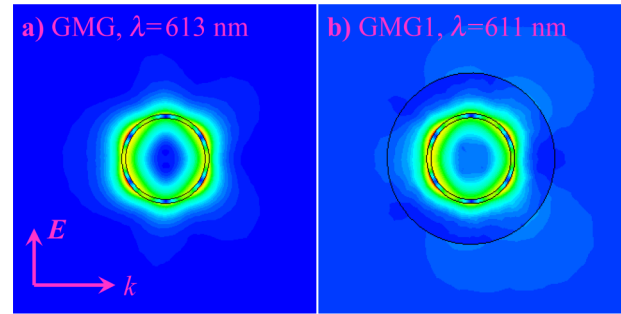

Figure 4 Comparison of the field enhancement $|\mathbf{E}|/\mathsf{E_0}$ between the GMG (a) and GMG1 (b) structures near the generation threshold of the $l = 3$ mode. In both cases, Johnson and Christy data are used for Ag, and $\varepsilon_G = 2.6\text{-}0.08i$. $a_1 = 50$ nm and $h_2 = 5$ nm for both structures, and $h_3 = 50$ nm in case of the GMG1 structure. The propagation direction and the polarization of the incident plane wave with the amplitude $\mathsf{E_0}$ are indicated in panel a).

with a GMG1 structure, where a gain containing core ($a_1 = 50$ nm) is covered by a silver shell ($h_2 = 5$ nm) and by a gain-shell ($h_3 = 50$ nm), followed by vacuum. We find that the difference is not substantial, because the relevant field structures are very similar near the metallic shell. This is illustrated in Fig. 4 for the $l = 3$ mode. For such a GMG structure, the enhanced field near the metallic shell initially decays on a length scale comparable to the radius of the inner core (50 nm). Figure 4b shows that for the GMG1 structure most of the enhanced field remains inside the 50 nm thick outer gain shell.

Numerical results for different core-shell structures at typical wavelengths are given in Table 2. The wavelengths, where spasing occurs for GMG and the GMG1 structures, are very similar, with better agreement for increasing multipolar number. The red-shift of the lower mode wavelengths of the GMG structure with respect to the GMG1 structure is due to the larger real part of

Table 2 Threshold gain $-\varepsilon''_G = -\varepsilon''_{thr}$ and the generation wavelengths λ_{thr} [nm] for the $l = 1$ to 5 modes of GMG, GMG1, GM2.6, 2.6GM, and GM1 structures obtained from the numerical solution of the exact analytical multi-shell Mie theory

	GMG			GMG1			GM2.6			2.6MG			GM1		
l	λ_{thr} [nm]	$-\varepsilon''_{\text{thr}}$	β_{thr} [cm⁻¹]	λ_{thr} [nm]	$-\varepsilon''_{\text{thr}}$	β_{thr} [cm⁻¹]	λ_{thr} [nm]	$-\varepsilon''_{\text{thr}}$	β_{thr} [cm⁻¹]	λ_{thr} [nm]	$-\varepsilon''_{\text{thr}}$	β_{thr} [cm⁻¹]	λ_{thr} [nm]	$-\varepsilon''_{\text{thr}}$	β_{thr} [cm⁻¹]
1	1012	0.3029	11645	937.1	0.1716	7133	995.2	1.3582	51552	1016	0.3873	14813	749.8	0.2921	15159
2	727.7	0.0531	2841	717.4	0.0410	2237	727.5	0.1624	8695	727.8	0.0788	4217	584.0	0.1124	7497
3	613.3	0.0719	4565	610.8	0.0714	4554	613.3	0.1901	12072	613.3	0.1155	7336	514.2	0.1179	8937
4	550.4	0.0834	5903	549.9	0.0839	5942	550.4	0.2075	14683	550.4	0.1394	9865	473.0	0.1317	10844
5	512.7	0.0772	5870	512.6	0.0773	5877	512.7	0.1862	14146	512.7	0.1320	10026	447.2	0.1107	9642

Ann. Phys. (Berlin) **528**, No. 3–4 (2016)

annalen
der **physik**

Original Paper

the dielectric function for the global background (2.6 vs. 1). The threshold gain is also remarkably similar for the GMG and the GMG1 case. For instance, in the case of the $l = 3$ mode (shown in Fig. 4), $-\varepsilon_G'' = 0.0719$ for GMG and $-\varepsilon_G'' = 0.0714$ in case of GMG1 (see colored entries in Table 2). In fact, the GMG1 structure shows slightly smaller threshold than the GMG structure. This is related to 2 factors: a) Small shift of the resonant wavelength towards locally better threshold conditions (see Ag curve in Fig. 1a near the green arrow). b) Lower radiative losses into the background with $\varepsilon_b = 1$ as compared to $\varepsilon_b \approx 2.6$ for the GMG case. To minimize the shift of the resonance, next we consider a GM2.6 structure, where only the inner core includes gain, followed by a metallic shell immersed in a passive matrix with the same, but purely real dielectric constant of $\varepsilon_3 = 2.6$. All geometrical dimensions are the same as for the GMG structure. In this case, the $l = 3$ mode needs a threshold gain of $-\varepsilon_G'' = 0.1901$, which is 2.64 times the gain required for the GMG structure. The complement, a 2.6MG structure (passive medium in the core with a metallic shell, embedded in an infinitely extended gain medium) requires $-\varepsilon_G'' = 0.1155$ for spasing, just 1.61 times the GMG gain. Finally, we consider a GM1 structure, *i.e.*, a gain core, covered with silver and put into vacuum. In this case, the $l = 3$ resonance is naturally blue-shifted due to the smaller real part of the outside dielectric. The required gain is now $-\varepsilon_G'' = 0.1179$. In fact, analyzing the expression (S.26) in Supp. Info. 6, one can show, that for a quasi-static metallic shell with $-\varepsilon_M' >> \varepsilon_{1,3}'$ in an asymmetric environment, $\varepsilon_{G,\text{eff}} = \varepsilon_1 + \frac{l+1}{l}\varepsilon_3$ plays the role of a dielectric function of a compound gain material. This observation elucidates why for GM2.6 thresholds are lower than for 2.6GM, and more so for lower multipoles. Similar comparisons as discussed for the $l = 3$ mode can be carried out for the other modes from $l = 1$ to 5, which are all shown in Table 2. These results suggest, that in the experimentally relevant case where several materials are involved (GM1, GMG1, as well as GM2.6 and 2.6GM structures), the threshold based on 2 materials provides the minimal values for the multiple-materials case. This is understandable, as the gainless materials can be considered as regions where gain was "switched off", which is likely to increase the threshold. In such comparisons, one should account for the spectral shift of the resonance (which changes the metal absorption), as well as changes in radiative losses in different backgrounds for larger structures.

The considered modes are the long-wavelength, charge-symmetric hybrid modes of the nano-shells [83]. The short-wavelength modes have significantly higher thresholds for nanoscale structures which we discuss here, while for large structures with thick shells they transform into the geometric resonances of the core, with low thresholds, similar to a spherical micro-lasers [47].

6 General eigenfunction expansion framework

The expansion of a scattering problem for an arbitrary composite particle in eigenfunctions of the Helmholtz equation is conceptually similar to the cases considered above. In most practical cases, the scattering cross-section can be written as a multipole expansion:

$$\sigma_{sca} = a^2 \sum_{l=1}^{\infty} \frac{(ka)^{4l} f_l}{\left| D_l(\varepsilon_M, \varepsilon_G, ka, \text{shape}) \right|^2} \qquad (14)$$

Here a loosely refers to the "size" of the structure, which shape may include several geometrical parameters. For example, an arbitrary ellipsoid is characterized by 3 axes, while a core-shell structure or torus has 2 spatial scales, but more complex cases obviously exist. The index l characterizes the multipole order, or, for more general asymmetric structures, the eigenfunctions of the structure. In the latter case, the power of ka in the numerator may differ. Denominators D_l in Eqns. (14) can be chosen dimensionless and their leading zero order terms are ka independent. Higher-order ka terms describe the so-called dynamic depolarization, radiative damping and inhomogeneity of polarization in the structure [80, 84]. For complex structures, they can include additional dielectric functions (for example ε_{host} for a core-shell structure in passive host medium). The functions f_l depend on similar arguments ($\varepsilon_M, \varepsilon_G,$ shape) but are usually independent from ka in the leading zero order. Mie expansion [85], or generalized Mie expansion for multi-shell structures [61, 64] have the form (14) and the size-expansions of their denominators are studied as examples in Supp. Info. 2 and 6.

Similarly to the equations (1)-(2), the condition $D_l = 0$ in (14) characterizes the generation threshold for the lth mode. Zero denominator allows the buildup of a finite polarization in the resonant mode from small spontaneous emission noise without an external field. The complex equation $D_l = 0$ allows one to find two real numbers, the threshold gain level $\varepsilon_G'' = \varepsilon_{thr}''$ and the generation wavelength λ_{thr}. Note, that the spectrum can contain several modes corresponding to the same l because of the ω-dependence of the dielectric functions ε_G and ε_M. One example is the splitting of the l-resonances in a core-shell particle [83].

Two final remarks: First, one can ask, if one can overcome the universal gain threshold by constructing quasi-static ensembles of metallic nanoparticles. In Supp. Info. 7 we elaborate on a two-particle geometry and show that the minimal gain requirement as given in Fig. 1 cannot be circumvented. Second, we note that some authors define the generation threshold as a gain for which the imaginary part of a complex eigenvalue ω of the electromagnetic problem for the structure disappears [19]. This definition is equivalent to the condition $D_l = 0$ in (14), which is used here and in some other works [50, 53], as outlined in Supp. Info. 8.

7 Conclusions

A spaser nanoscopically confined in all 3 dimensions is a truly nano-scale source of coherent electromagnetic fields in the visible and near IR. The main difficulty in its practical realization lies in metal absorption, which necessitates high concentration of the active (lasing) agents, *e.g.*, fluorescent dye molecules. In this contribution, we have investigated the threshold gain necessary for spasing and found that for the quasi-static spasers it depends only on the materials involved. As the materials' parameters show dispersion, the lasing threshold shows a dispersion as well; however various spasers, utilizing different nanoparticle shapes and modes, but generating on the same wavelength, have equal thresholds. Specifically, there exists a global minimum of required gain for each combination of materials, which, however, does not depend on the specific shape, multipolar spasing mode or even arrangements involving several particles, such as nanoparticle dimers. Geometric design and choice of multipole order can only shift the plasmonic resonance towards the wavelength of minimal gain. This wavelength of lowest spasing threshold is determined by the minimum of the metal $-\varepsilon_M''/\varepsilon_M'$ ratio, because the dispersion of this ratio is typically much larger than the dispersion of the real part of the gain material's dielectric constant. In addition, low values of the host dielectric function ε_G' decrease threshold gain values.

These general statements follow from the classical, macroscopic electrodynamic expressions for scattering coefficients, without invoking quantum mechanical arguments. Spasing threshold corresponds to the zero of the denominator in the corresponding scattering coefficient; this holds also for systems with retardation. The results are illustrated by the examples of dipolar modes of silver spheroids and multipoles of core-shell structures for which thresholds are calculated explicitly for a broad range of sizes. Our results show how the retardation increases spaser thresholds due to radiative losses. In addition, damping due to surface scattering of the conduction electrons (not included into bulk values of the dielectric constants used here) will increase the gain threshold. Further, the ideal limit for the minimal threshold (11) holds in the absence of quenching of chromophores via energy transfer to the plasmonic structures. It can bleach the population inversion within about 5 nm near the metal structures [86–88], and/or funnel the pumping energy into the undesirable, spectrally overlapping modes, resulting in additional losses and detrimental mode competition. The limit (11) can however be approached either with fs optical pumping, or in case of multipolar modes of a moderately large ($\sim$50-100 nm) quasi-static structures, where the relative importance of quenching with respect to scattering is smaller. Femtosecond pumping, if strong enough everywhere, will invert all available chromophores, and make the gain, defined as ε_G'', spatially homogeneous irrespectively of the distribution of the pumping intensity and/or Purcell-enhanced relaxation rate into the resonant and even non-resonant plasmonic modes.

As a qualitative recipe, one can suggest that: a) if the wavelength of minimal gain can be realized with different geometries and/or multipolar orders, the solution with the smallest surface to volume ratio should be preferred; b) higher order modes, despite being "dark" or "non-radiative" under normal conditions, often become advantageous for the generation, as they allow larger structures, where the boundary losses and quenching are less prominent.

Minimal threshold gain values translate into dye concentrations close to those available with commercial dye-doped polymers, where pulsed optical pumping is not expected to cause thermal issues. At the same time, the so far experimentally explored geometries and material combinations are not always optimal. In particular, minimal conditions for Ag and Au nanoparticles suggest structures with substantial geometric aspect ratio, which significantly deviate from a sphere, in order to red-shift the plasmon resonance into the region of lower thresholds. For Ag, the favorable wavelength range spans 730–1140 nm and requires gain values of $-\varepsilon_G'' \sim 0.03$ or an amplification of $\beta \sim 10^3 \; cm^{-1}$ only. The values for Au are about an order of magnitude larger.

Key words. localized surface plasmon, laser threshold, plasmonics, retardation, Spaser.

Ann. Phys. (Berlin) **528**, No. 3–4 (2016)

annalen
der **physik**

References

[1] G. A. Plotz, H. J. Simon and J. M. Tucciarone, J. Opt. Soc. Am. **69** (3), 419–421 (1979).

[2] A. N. Sudarkin and P. A. Demkovich, Sov. Phys. Tech. Phys. **34** (7), 764–766 (1989).

[3] N. M. Lawandy, Appl. Phys. Lett. **85** (21), 5040–5042 (2004).

[4] D. J. Bergman and M. I. Stockman, Phys. Rev. Lett. **90** (2), 027402 (2003).

[5] M. I. Stockman, J. Opt. Ukr. **12** (2), 024004 (2010).

[6] Y. E. Lozovik, I. A. Nechepurenko, A. V. Dorofeenko, E. S. Andrianov and A. A. Pukhov, Phys. Lett. A **378** (9), 723–727 (2014).

[7] S. A. Ramakrishna and J. B. Pendry, Phys. Rev. B **67** (20), 201101 (2003).

[8] T. A. Klar, A. V. Kildishev, V. P. Drachev and V. M. Shalaev, IEEE J Sel Top Quant. Electron **12** (6), 1106–1115 (2006).

[9] M. Wegener, J. L. Garcia-Pomar, C. M. Soukoulis, N. Meinzer, M. Ruther and S. Linden, Opt. Express **16** (24), 19785–19798 (2008).

[10] Y. Sivan, S. M. Xiao, U. K. Chettiar, A. V. Kildishev and V. M. Shalaev, Opt. Express **17** (26), 24060–24074 (2009).

[11] A. Fang, T. Koschny, M. Wegener and C. M. Soukoulis, Phys. Rev. B **79** (24), 241104 (2009).

[12] E. Plum, V. A. Fedotov, P. Kuo, D. P. Tsai and N. I. Zheludev, Opt. Express **17** (10), 8548–8551 (2009).

[13] S. M. Xiao, V. P. Drachev, A. V. Kildishev, X. J. Ni, U. K. Chettiar, H. K. Yuan and V. M. Shalaev, Nature **466** (7307), 735–738 (2010).

[14] N. Meinzer, M. Ruther, S. Linden, C. M. Soukoulis, G. Khitrova, J. Hendrickson, J. D. Olitzky, H. M. Gibbs and M. Wegener, Opt. Express **18** (23), 24140–24151 (2010).

[15] S. Wuestner, A. Pusch, K. L. Tsakmakidis, J. M. Hamm and O. Hess, Phys. Rev. Lett. **105** (12), 127401 (2010).

[16] X. J. Ni, S. Ishii, M. D. Thoreson, V. M. Shalaev, S. H. Han, S. Lee and A. V. Kildishev, Opt. Express **19** (25), 25242–25254 (2011).

[17] O. Hess, J. B. Pendry, S. A. Maier, R. F. Oulton, J. M. Hamm and K. L. Tsakmakidis, Nat. Mater. **11** (7), 573–584 (2012).

[18] I. E. Protsenko, A. V. Uskov, O. A. Zaimidoroga, V. N. Samoilov and E. P. O'Reilly, Phys. Rev. A **71** (6), 063812 (2005).

[19] M. A. Noginov, G. Zhu, A. M. Belgrave, R. Bakker, V. M. Shalaev, E. E. Narimanov, S. Stout, E. Herz, T. Suteewong and U. Wiesner, Nature **460** (7259), 1110-U1168 (2009).

[20] X. G. Meng, A. V. Kildishev, K. Fujita, K. Tanaka and V. M. Shalaev, Nano. Lett. **13** (9), 4106–4112 (2013).

[21] M. T. Hill, Y. S. Oei, B. Smalbrugge, Y. Zhu, T. De Vries, P. J. Van Veldhoven, F. W. M. Van Otten, T. J. Eijkemans, J. P. Turkiewicz, H. De Waardt, E. J. Geluk, S. H. Kwon, Y. H. Lee, R. Nötzel and M. K. Smit, Nat. Photon. **1** (10), 589–594 (2007).

[22] N. I. Zheludev, S. L. Prosvirnin, N. Papasimakis and V. A. Fedotov, Nat. Photon. **2** (6), 351–354 (2008).

[23] R. F. Oulton, V. J. Sorger, T. Zentgraf, R. M. Ma, C. Gladden, L. Dai, G. Bartal and X. Zhang, Nature **461** (7264), 629–632 (2009).

[24] M. P. Nezhad, A. Simic, O. Bondarenko, B. Slutsky, A. Mizrahi, L. A. Feng, V. Lomakin and Y. Fainman, Nat. Photon. **4** (6), 395–399 (2010).

[25] C. Y. Lu, S. W. Chang, S. L. Chuang, T. D. Germann and D. Bimberg, Appl. Phys. Lett. **96** (25), 251101 (2010).

[26] S. H. Kwon, J. H. Kang, C. Seassal, S. K. Kim, P. Regreny, Y. H. Lee, C. M. Lieber and H. G. Park, Nano. Lett. **10** (9), 3679–3683 (2010).

[27] C. Y. Wu, C. T. Kuo, C. Y. Wang, C. L. He, M. H. Lin, H. Ahn and S. Gwo, Nano. Lett. **11** (10), 4256–4260 (2011).

[28] R. M. Ma, R. F. Oulton, V. J. Sorger, G. Bartal and X. A. Zhang, Nat. Mater. **10** (2), 110–113 (2011).

[29] Y. J. Lu, J. Kim, H. Y. Chen, C. H. Wu, N. Dabidian, C. E. Sanders, C. Y. Wang, M. Y. Lu, B. H. Li, X. G. Qiu, W. H. Chang, L. J. Chen, G. Shvets, C. K. Shih and S. Gwo, Science **337** (6093), 450–453 (2012).

[30] K. Ding, Z. C. Liu, L. J. Yin, M. T. Hill, M. J. H. Marell, P. J. van Veldhoven, R. Noetzel and C. Z. Ning, Phys. Rev. B **85** (4), 041301 (2012).

[31] Q. Gu, J. S. T. Smalley, M. P. Nezhad, A. Simic, J. H. Lee, M. Katz, O. Bondarenko, B. Slutsky, A. Mizrahi, V. Lomakin and Y. Fainman, Adv. Opt. Photon. **6** (1), 1–56 (2014).

[32] A. Tredicucci, C. Gmachl, F. Capasso, A. L. Hutchinson, D. L. Sivco and A. Y. Cho, Appl. Phys. Lett. **76** (16), 2164–2166 (2000).

[33] J. Seidel, S. Grafstrom and L. Eng, Phys. Rev. Lett. **94** (17), 177401 (2005).

[34] P. Berini and I. De Leon, Nat. Photon. **6** (1), 16–24 (2012).

[35] R. A. Flynn, C. S. Kim, I. Vurgaftman, M. Kim, J. R. Meyer, A. J. Makinen, K. Bussmann, L. Cheng, F. S. Choa and J. P. Long, Opt. Express **19** (9), 8954–8961 (2011).

[36] I. E. Protsenko, Phys. Usp. **55** (10), 1040–1046 (2012).

[37] A. S. Rosenthal and T. Ghannam, Phys. Rev. A **79** (4), 043824 (2009).

[38] X. L. Zhong and Z. Y. Li, Phys. Rev. B **88** (8), 085101 (2013).

[39] A. A. Lisyansky, E. S. Andrianov, A. V. Dorofeenko, A. A. Pukhov and A. P. Vinogradov, Plasmonics: Metallic Nanostructures and Their Optical Properties X **8457**, 84570X (2012).

[40] E. S. Andrianov, A. A. Pukhov, A. V. Dorofeenko, A. P. Vinogradov and A. A. Lisyansky, Opt. Express **19** (25), 24849–24857 (2011).

[41] N. Arnold, L. J. Prokopeva and A. V. Kildishev, Annual Rev. Prog. Appl. Comp. Electromagnetics **29**, 771–776 (2013).

[42] X. F. Li and S. F. Yu, Opt. Lett. **35** (15), 2535–2537 (2010).

[43] S. Y. Liu, J. F. Li, F. Zhou, L. Gan and Z. Y. Li, Opt. Lett. **36** (7), 1296–1298 (2011).

[44] S. D. Campbell and R. W. Ziolkowski, Adv. Opto. Electron **2012**, 368786 (2012).

[45] M. Cao, M. Wang and N. Gu, Plasmonics **7** (2), 347–351 (2012).

[46] J. P. Geng, R. W. Ziolkowski, R. H. Jin and X. L. Liang, Radio Sci. **47**, RS2013 (2012).

[47] J. Pan, Z. Chen, J. Chen, P. Zhan, C. J. Tang and Z. L. Wang, Opt. Lett. **37** (7), 1181–1183 (2012).

[48] H. P. Zhang, J. Zhou, W. B. Zou and M. He, J. Appl. Phys. **112** (7) (2012).

[49] E. S. Andrianov, D. G. Baranov, A. A. Pukhov, A. V. Dorofeenko, A. P. Vinogradov and A. A. Lisyansky, Opt. Express **21** (11), 13467–13478 (2013).

[50] N. Arnold, B. Y. Ding, C. Hrelescu and T. A. Klar, Beilstein J. Nanotech **4**, 974–987 (2013).

[51] D. G. Baranov, E. S. Andrianov, A. P. Vinogradov and A. A. Lisyansky, Opt. Express **21** (9), 10779–10791 (2013).

[52] P. Ding, J. N. He, J. Q. Wang, C. Z. Fan, G. W. Cai and E. J. Liang, J. Opt. Ukr. **15** (10), 105001 (2013).

[53] X. G. Meng, U. Guler, A. V. Kildishev, K. Fujita, K. Tanaka and V. M. Shalaev, Sci. Rep. **3**, 1241 (2013).

[54] W. R. Zhu, M. Premaratne, S. D. Gunapala, G. P. Agrawal and M. I. Stockman, J. Opt. Ukr. **16** (7) (2014).

[55] J. Song, Y. L. Tian, S. Ye, L. C. Chen, X. Peng and J. L. Qu, J Lightwave Technol **33** (15), 3215–3223 (2015).

[56] A. Y. Smuk and N. M. Lawandy, Appl. Phys. B **84** (1-2), 125–129 (2006).

[57] J. A. Gordon and R. W. Ziolkowski, Opt. Express **15** (5), 2622–2653 (2007).

[58] S. Arslanagic and R. W. Ziolkowski, IEEE J Sel Top Quant. Electron **19** (3), 4800506 (2013).

[59] S. Arslanagic and R. W. Ziolkowski, Appl. Phys. A **103** (3), 795–798 (2011).

[60] S. Arslanagic and R. W. Ziolkowski, J. Opt. Ukr. **12** (2), 024014 (2010).

[61] M. Quinten, Optical properties of nanoparticle systems: Mie and beyond. (Wiley-VCH, Weinheim, Germany, 2011).

[62] F. Wang and Y. R. Shen, Phys. Rev. Lett. **97** (20), 206806 (2006).

[63] M. I. Stockman, Opt. Express **19** (22), 22029–22106 (2011).

[64] U. Kreibig and M. Vollmer, Optical properties of metal clusters. (Springer, Berlin, 1995).

[65] L. D. Landau, L. P. Pitaevskii and E. M. Lifshitz, Electrodynamics of continuous media, 2nd ed. (Pergamon, Oxford, 1984).

[66] N. Arnold, K. Piglmayer, A. V. Kildishev and T. A. Klar, Opt. Mater. Express **5** (11), 2546–2577 (2015).

[67] X. G. Meng, U. Guler, A. V. Kildishev, K. Fujita, K. Tanaka and V. M. Shalaev, Sci. Rep-Uk **3** (2013).

[68] P. Ding, J. N. He, J. Q. Wang, C. Z. Fan, G. W. Cai and E. J. Liang, J. Opt. **15** (10) (2013).

[69] A. E. Siegman, Lasers. (University Science Books, Mill Valley, Calif., 1986).

[70] N. V. Karlov, Lectures on quantum electronics. (CRC Press, Boca Raton, Fla., 1993).

[71] P. B. Johnson and R. W. Christy, Phys. Rev. B **6** (12), 4370–4379 (1972).

[72] J. B. Khurgin and G. Sun, Nat. Photon. **8** (6), 468–473 (2014).

[73] J. B. Khurgin and G. Sun, Opt. Express **20** (14), 15309–15325 (2012).

[74] R. Hillenbrand, T. Taubner and F. Keilmann, Nature **418** (6894), 159–162 (2002).

[75] J. D. Caldwell, O. J. Glembocki, Y. Francescato, N. Sharac, V. Giannini, F. J. Bezares, J. P. Long, J. C. Owrutsky, I. Vurgaftman, J. G. Tischler, V. D. Wheeler, N. D. Bassim, L. M. Shirey, R. Kasica and S. A. Maier, Nano. Lett. **13** (8), 3690–3697 (2013).

[76] T. Wang, P. N. Li, B. Hauer, D. N. Chigrin and T. Taubner, Nano. Lett. **13** (11), 5051–5055 (2013).

[77] M. A. Noginov, G. Zhu, M. Bahoura, J. Adegoke, C. Small, B. A. Ritzo, V. P. Drachev and V. M. Shalaev, Appl. Phys. B **86** (3), 455–460 (2007).

[78] M. A. Noginov, G. Zhu, M. Bahoura, J. Adegoke, C. E. Small, B. A. Ritzo, V. P. Drachev and V. M. Shalaev, Opt. Lett. **31** (20), 3022–3024 (2006).

[79] H. Kuwata, H. Tamaru, K. Esumi and K. Miyano, Appl. Phys. Lett. **83** (22), 4625–4627 (2003).

[80] A. Moroz, J. Opt. Soc. Am. B **26** (3), 517–527 (2009).

[81] G. Raschke, PhD thesis, Ludwig–Maximilians–Universität München, 2005.

[82] H. O. Hagenvik, M. E. Malema and J. Skaar, Phys. Rev. A **91** (4) (2015).

[83] E. Prodan, C. Radloff, N. J. Halas and P. Nordlander, Science **302** (5644), 419–422 (2003).

[84] M. Meier and A. Wokaun, Opt. Lett. **8** (11), 581–583 (1983).

[85] M. Born and E. Wolf, Principles of optics: electromagnetic theory of propagation, interference and diffraction of light, 7th expanded ed. (Cambridge University Press, Cambridge, 1999).

[86] A. Moroz, Opt. Commun. **283** (10), 2277–2287 (2010).

[87] G. C. des Francs, A. Bouhelier, E. Finot, J. C. Weeber, A. Dereux, C. Girard and E. Dujardin, Opt. Express **16** (22), 17654–17666 (2008).

[88] R. Ruppin, J. Chem. Phys. **76** (4), 1681–1684 (1982).

Supporting Information

Additional supporting information may be found in the online version of this article at the publisher's website.

Article type: Original Paper

Supporting Information,

Minimal Spaser Threshold within Electrodynamic Framework: Shape, Size and Modes

Nikita Arnold[1,2,], Calin Hrelescu[1], and Thomas A. Klar[1]*

* Corresponding author: email: nikita.arnold@jku.at

[1] Institute of Applied Physics, Johannes Kepler University Linz, Altenbergerstraße 69, 4040 Linz, Austria
[2] Soft Matter Physics, Johannes Kepler University Linz, Altenbergerstraße 69, 4040 Linz, Austria

Supp. Info. 1. Depolarization factors for spheroids

Let us consider ellipsoids of revolution (spheroids), rotationally symmetric about the *z*-axis and with a semi-axis length *c*. Two other semi-axes are *a*=*b*, which we will refer to as *a*. The semi-axis along the field polarization direction is denoted as a_E. Depending on the irradiation geometry $a_E = c$, or $a_E = a$. Such a spheroid has the volume

$$V = \frac{4\pi}{3}a^2 c , \tag{S.1}$$

and the *static* depolarization factors *L* involving the eccentricity *e* are given by:[1]

$$e = \begin{cases} \sqrt{1-a^2/c^2} & \text{for prolate } a < c \\ \sqrt{1-c^2/a^2} & \text{for oblate } c < a \end{cases}$$

$$L_z = e^{-2} \cdot \begin{cases} (1-e^2)\left(\frac{1}{2e}\ln\frac{1+e}{1-e}-1\right) & \text{for prolate } a < c \\ 1-e^{-1}\sqrt{1-e^2}\arcsin e & \text{for oblate } c < a \end{cases} \tag{S.2}$$

$$L_{x,y} = \frac{1-L_z}{2}$$

The depolarization factor *L* should be taken along the electric field direction.

Supp. Info. 2. Multipoles of spherical particles, including retardation correction

For illustrative purposes, let us consider the resonant denominators of the multipole expansion (14), including the retardation corrections up to the first meaningful order, for a sphere with the vacuum Mie parameter $q = ka_1$, a_1 being sphere radius. They are obtained from the Taylor expansion of the classical Mie formulas [1-3] into the size parameter q. We choose the form of denominator most convenient for the studies of the near-threshold behavior (hence proportionality sign instead of equality). Subscript 1 refers to the sphere, 2 to the ambient medium.

$$
D_l \sim l\varepsilon_1 + (l+1)\varepsilon_2 + \frac{q^2}{2}(\varepsilon_2 - \varepsilon_1)\left[\frac{l\varepsilon_1}{2l+3} + \frac{(l+1)\varepsilon_2}{2l-1} + O(q^2)\right] +
$$
$$
iq^{2l+1}(\varepsilon_2 - \varepsilon_1)\left[\frac{(l+1)\varepsilon_2^{l+1/2}}{(2l-1)!!(2l+1)!!} + O(q^2)\right]
$$
(S.3)

Terms in the first row are responsible for the spectral shifts of the resonances. Their origin lies in the dynamic depolarization and inhomogeneity of polarization over the sphere size. Terms in the second row are associated with the multipole radiative losses. All corrections disappear for $\varepsilon_1 = \varepsilon_2$. For higher multipoles the shift remains quadratic in q, while the radiative losses decrease as q^{2l+1} (as $q \ll 1$).

Let us review the origin of the radiative losses for the dipolar mode. We omit dimensionless factors related to shape and ε everywhere. The energy W of the oscillating dipole d can be estimated from its volume V, associated field E and polarization P as:

$$
W \sim V\,E^2 \sim V\,P^2 \sim d^2/V
$$
(S.4)

The radiated power I is [4]:

$$
I \sim \ddot{d}^2/c^3 \sim \omega^4 d^2/c^3 \sim \omega k^3 d^2
$$
(S.5)

Here c and k are the speed of light and wavenumber in vacuum. The radiative decay rate is the ratio of I/W and is of the order of

$$
\gamma_{rad} \sim I/W \sim \omega k^3 V
$$
(S.6)

Thus, *dimensionless* radiative corrections to all physical quantities should be of the order of

$k^3 V \sim q^3$. This is indeed the case in the expression (S.3) for the dipolar mode with $l=1$.

Similar considerations can be applied to the multipoles. The Eq. (S.3) shows that the

corresponding corrections scale as q^{2l+1}, which suggests radiative damping of

$$\gamma_{rad} \sim \omega q^{2l+1} \sim \omega (kV^{1/3})^{2l+1} \tag{S.7}$$

Formulas similar to (S.3) can be found in the literature. In [5, 6], Appendix A of Ref. [7], and

chapter 5 of ref. [8], different approximations are discussed, although apart from Ref. [6], for

the dipolar mode only. As we are interested in the threshold, we Taylor-expand the

denominator only, while for the studies of cross-sections far from the threshold one has to

expand the numerator of the Mie coefficients as well. The last term in (S.7), which results in

(S.8) below, agrees with the effective multipolar polarizability correction from Ref. [9].

For real dielectric functions the particle acquires an effective imaginary part of ε_1 due to

(multipole) radiation:

$$\varepsilon''_{1eff} = q^{2l+1} \frac{(l+1)(\varepsilon_2 - \varepsilon_1)\varepsilon_2^{l+1/2}}{l(2l-1)!!(2l+1)!!} \tag{S.8}$$

Supp. Info. 3. Optimal threshold conditions for Drude metal

Let us consider a Drude metal with the dielectric function

$$\varepsilon_M = \varepsilon_\infty - \frac{\omega_p^2}{\omega(\omega + i\gamma)} \tag{S.9}$$

The gain material shall be characterized by the constant dielectric function

$$\varepsilon_G = \varepsilon'_G + i\varepsilon''_G \tag{S.10}$$

For a given shape factor N, we can resolve the general conditions (11) and find the generation

frequency and gain:

$$\omega = \gamma\sqrt{\frac{N\omega_p^2/\gamma^2}{\varepsilon_G' + N\varepsilon_\infty} - 1} \approx \frac{\omega_p\sqrt{N}}{\sqrt{\varepsilon_G' + N\varepsilon_\infty}}, \quad -\varepsilon_G'' = \frac{\varepsilon_G' + N\varepsilon_\infty}{\sqrt{\dfrac{N\omega_p^2/\gamma^2}{\varepsilon_G' + N\varepsilon_\infty} - 1}} \approx \frac{\gamma(\varepsilon_G' + N\varepsilon_\infty)^{3/2}}{\omega_p\sqrt{N}} \qquad \text{(S.11)}$$

The second approximations refer to the case of weak damping, $\varepsilon_\infty\gamma^2 \ll \omega_p^2$. To find the minimal gain, we can either minimize the 2nd of these expressions as a function of N, or use the 2nd equality from (11), which for Drude metal (S.9) reads

$$-\varepsilon_G'' = \varepsilon_G' \frac{\omega_p^2\gamma/\omega}{\omega_p^2 - \varepsilon_\infty(\omega^2 + \gamma^2)}, \qquad \text{(S.12)}$$

and minimize it with respect to ω. The origin of the minimum can be understood as a tradeoff between the two factors: in the UV the metal is not metallic enough, while in the IR the losses become too high. This yields a set of optimal parameters:

$$w = \frac{\omega_p^2}{\varepsilon_\infty\gamma^2}, \quad N_{min} = \frac{\varepsilon_G'}{2\varepsilon_\infty}\left(\frac{w+2}{w-1}\right) \overset{w\gg1}{\approx} \frac{\varepsilon_G'}{2\varepsilon_\infty}$$

$$\omega_{min} = \gamma\frac{(w-1)^{1/2}}{\sqrt{3}} \overset{w\gg1}{\approx} \frac{\omega_p}{\sqrt{3\varepsilon_\infty}}, \quad -\varepsilon_{min}'' = \frac{3\sqrt{3}}{2}\frac{\varepsilon_G'w}{(w-1)^{3/2}} \overset{w\gg1}{\approx} \frac{3\sqrt{3}}{2}\frac{\gamma}{\omega_p}\varepsilon_G'\varepsilon_\infty^{1/2} \qquad \text{(S.13)}$$

For brevity, we introduced a dimensionless parameter w characterizing the quality of plasma oscillations. Its value is usually high, and the last approximations in (S.13) correspond to the typical case $w\gg1$. Note, that in the lowest order, changes in γ (e.g., due to boundary losses) do not change N_{min} and ω_{min}, but linearly increase the threshold $-\varepsilon_{min}$.

Let us consider the case of Ag in a polymer matrix with $\varepsilon_G' = 2.6$ studied throughout this paper. For the Drude values of Ag we have chosen the following consensus average between the refs. [10-12] with the real part of the high frequency interband Lorentzian incorporated into ε_∞ (matching in the middle of the VIS range):

$\omega_p = 1.39\times10^{16}$ rad/s, $\gamma = 3.34\times10^{13}$ s^{-1}, $\varepsilon_\infty = 4.4$. These parameters result in the following optimal values for silver calculated with the first (full) formulas (S.13):

$$w = 3.9\times10^4 \gg 1, \; N_{min} \approx 0.30, \; \lambda_{min} \approx 492 \text{ nm}, \; -\varepsilon_{min}'' \approx 0.034 \qquad \text{(S.14)}$$

These results semi-quantitatively agree with those in Table 1, which are based on the experimental ε_{Ag}. The discrepancies are due to the deviations from the Drude behavior for silver. In fact, λ_{min} is shifted towards IR for experimental ε_{Ag} values, because the absorption of silver is anomalously low there, as compared to the Drude values. The Au data are obtained in a similar way from [12] and are valid above about 450 nm only. For $\varepsilon_G' = 2.6$ we find:

$$\omega_p = 1.36 \times 10^{16}\,\text{rad/s}, \quad \gamma = 1.67 \times 10^{14}\,\text{s}^{-1}, \quad \varepsilon_\infty = 9.5$$
$$w = 698 \gg 1, \quad N_{min} \approx 0.14, \quad \lambda_{min} \approx 739\,\text{nm}, \quad -\varepsilon_{min}'' \approx 0.26$$
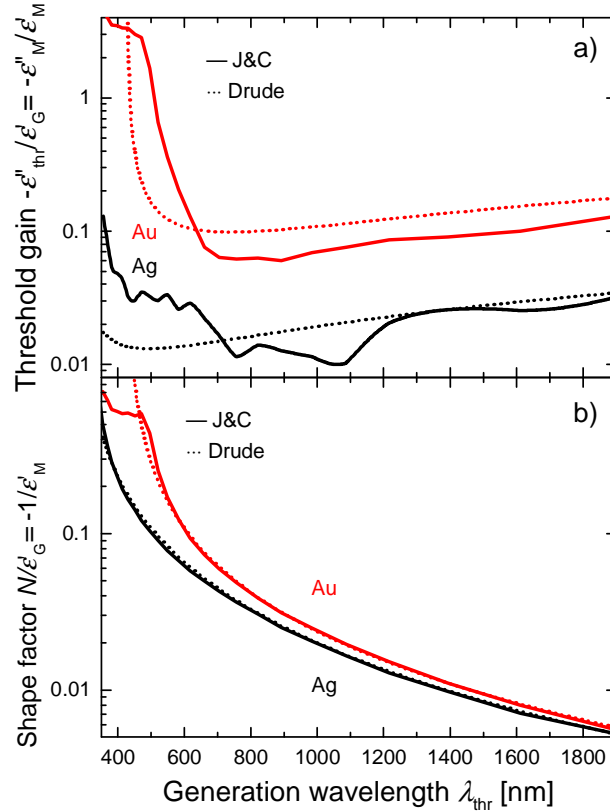
(S.15)

Figure SI.1. Quasi-static threshold parameters calculated with the Johnson & Christy values (J&C, solid curves) and with the Drude parameters given in the text (dotted curves) for Ag (black) and Au (red). a) The normalized threshold gain $-\varepsilon_M''/\varepsilon_M'$ vs. generation wavelength λ_{thr}, similar to the solid curves in the Fig. 1a of the main text. The threshold gain $-\varepsilon_G''$ can be obtained by multiplying these data with the ε_G' of the gain material. b) The corresponding $-1/\varepsilon_M'$ values, equal to the normalized shape factor N/ε_G' for this wavelength. Both ordinates have logarithmic scales.

These results are in good agreement with the experimental ε_{Au} data in Table 1. The formulas

(S.13) provide guidelines for the influence of different factors on minimal parameters. Figure

SI.1 compares the universal quasi-static threshold parameters calculated with Johnson and

Christy and the Drude dielectric functions. The agreement is better agreement for the shape

factor N in Fig. SI.1b because it depends only on ε'_M, where J&C data are in better agreement

with Drude than for ε''_M.

Supp. Info. 4. Generation frequency and threshold for a Lorentzian gain of finite width

In this section, gain material shall be characterized by a Lorentzian of finite FWHM γ_L:

$$\varepsilon_G = \varepsilon_h - \frac{\varepsilon_L \gamma_L / 2}{(\omega_L - \omega) - i\gamma_L / 2} = \varepsilon_h - \varepsilon_L \underbrace{\frac{[(\omega_L - \omega) + i\gamma_L / 2]\gamma_L / 2}{(\omega_L - \omega)^2 + (\gamma_L / 2)^2}}_{L = L' + iL''} \tag{S.16}$$

With these notations $\varepsilon_L > 0$ characterizes gain strength, and the Lorentzian profile L is

defined such, that in the center of the line $L''(\omega_L) = 1$, and correspondingly $\varepsilon''_G(\omega_L) = -\varepsilon_L < 0$.

Because now both ε_G and ε_M have a spectral dependence, the generation will not always

take place in the center of the Lorentzian line, where ε''_G has its maximum, and $\varepsilon'_G = \varepsilon_h$. Our

goal is to find the generation frequency and necessary threshold gain level ε_L. The general

threshold conditions (11) remain valid, and can be written in the form:

$$D = \underbrace{\varepsilon_h - \varepsilon_L (L' + iL'')}_{\varepsilon_G} + N(\varepsilon'_M + i\varepsilon''_M) = 0 \Rightarrow$$

$$N = \frac{\varepsilon_h L''}{\varepsilon''_M L' - \varepsilon'_M L''} = \frac{-\varepsilon_h}{\varepsilon'_M + \varepsilon''_M \delta}, \quad \varepsilon_L = \frac{N\varepsilon''_M}{L''} = \frac{\varepsilon_h \varepsilon''_M}{\varepsilon''_M L' - \varepsilon'_M L''} = \frac{-\varepsilon_h \varepsilon''_M [1 + \delta^2]}{\varepsilon'_M + \varepsilon''_M \delta} \tag{S.17}$$

where $\delta \equiv \dfrac{\omega - \omega_L}{\gamma_L / 2}$

Similarly to (11), for a given shape factor N, the 1st of these conditions defines the generation

frequency, and the 2nd defines the threshold gain ε_L. In general, these equations can be

resolved only numerically, as $\varepsilon''_M, \varepsilon'_M, \delta$, and even ε_h may depend on ω. For a flat gain

$\gamma_L \to \infty$, $\delta \to 0$, and we recover the simple expressions (11) and the corresponding minimal

conditions. Moreover, for each desired generation frequency ω, one can always tune the

particle shape such that $N = -\varepsilon_h / \varepsilon'_M$. In this case relations (S.17) imply that $\delta = 0$, and

$\varepsilon_L = -\varepsilon_h \varepsilon''_M / \varepsilon'_M$. This corresponds to the tuning of plasmonic resonance to the center of the

emission line. The formulas again coincide with (11), and the global minimal conditions still

hold.

With detuning between the emission line ω_L and plasmon resonance ω_{res}, the 1st of the

conditions (S.17) is similar to that for the laser generation frequency ω, which occurs between

the mode of the "cold" (gain-less) resonator and gain emission line [13, 14]:

$$(\omega - \omega_{res}) \cdot Q_{res} = (\omega_L - \omega) \cdot Q_L \tag{S.18}$$

Here Q are the corresponding quality factors. For the emission line $Q_L = \omega_L / \gamma_L$, while the

properties of the resonator mode are implicitly defined by N and the spectral behavior of

$\varepsilon''_M, \varepsilon'_M$ and, if relevant, ε_h. The position of the "cold" resonance ω_{res} is given by the

minimum of the denominator, while its FWHM γ_{res} corresponds to the twofold increase of

the denominator from its minimal value at resonance:

$$
\begin{aligned}
&\left. \varepsilon_h + N\varepsilon'_M \right|_{\omega_{res}} = 0 \\
&\left. \varepsilon_h + N\varepsilon'_M \right|_{\omega_{res} \pm \gamma_{res}/2} \approx \left. N\varepsilon''_M \right|_{\omega_{res}}
\end{aligned}
\tag{S.19}
$$

A Taylor expansion of the 2nd term in the last equation, assuming weak variations in other

quantities, yields:

$$\gamma_{res} \approx \left. \frac{2\varepsilon''_M}{|\partial \varepsilon'_M / \partial \omega|} \right|_{\omega_{res}}, \quad Q_{res} \equiv \frac{\omega_{res}}{\gamma_{res}} = \left. \frac{\omega |\partial \varepsilon'_M / \partial \omega|}{2\varepsilon''_M} \right|_{\omega_{res}} \tag{S.20}$$

We again assume the strongest variation due to ε'_M, and $\partial\varepsilon'_M / \partial\omega\big|_{\omega_{res}} > 0$ (otherwise in the

final result one should multiply γ_{res} by the $\mathrm{sign}[\partial\varepsilon'_M / \partial\omega\big|_{\omega_{res}}]$). Then the 1$^{\mathrm{st}}$ of the conditions

(S.17) can be transformed as follows:

$$
\delta \equiv \frac{\omega - \omega_L}{\gamma_L / 2} = \frac{\varepsilon_h + N\varepsilon'_M}{-N\varepsilon''_M}\bigg|_\omega \approx \overbrace{\frac{\varepsilon_h + N\varepsilon'_M}{-N\varepsilon''_M}\bigg|_{\omega_{res}}}^{0} - \frac{\partial\varepsilon'_M / \partial\omega}{\varepsilon''_M}\bigg|_{\omega_{res}} (\omega - \omega_{res}) \Rightarrow
$$
$$
\frac{\omega - \omega_L}{\gamma_L} = -\frac{\partial\varepsilon'_M / \partial\omega}{2\varepsilon''_M}\bigg|_{\omega_{res}} (\omega - \omega_{res}) \Rightarrow \omega = \frac{\gamma_{res}\omega_L + \gamma_L\omega_{res}}{\gamma_L + \gamma_{res}}
$$

(S.21)

Within resonant approximation $\omega \approx \omega_L \approx \omega_{res}$, this coincides with (S.18). For good Drude

metal, (S.20) results in $\gamma_{res} \approx \gamma$, $Q_{res} \approx \omega / \gamma$, and (S.21) reproduces the result obtained in [15]

from the quantum-mechanical considerations. For realistic numbers, when the detuning

$|\lambda_L - \lambda_{res}| < \Delta\lambda_L \sim 50\ \mathrm{nm}$, λ_{thr} lies between λ_L and λ_{res}, while ε_L may increase by about

~20% from the on-resonance value. If the shape factor N is known, the exact numbers can be

obtained numerically from (S.17), which has larger applicability than the subsequent

approximate formulas.

Supp. Info. 5. Minimal threshold conditions for Lorentzian absorber (polar crystals in the IR)

Conventional plasmonics uses metals as the materials with a negative real part of the

dielectric function ε'. Another possibility to obtain $\varepsilon' < 0$ is to use the region near a strong

(Lorentzian) absorption line, for example due to optical phonons in polar dielectric crystals

[16, 17]. Such phonon-polariton resonances are usually in the IR. For reference purposes, we

give here the optimal conditions similar to (S.13), if the absorber (index A) has a Lorentzian

line profile instead of a Drude dispersion. In the resonant approximation, this profile can be

described by

$$
\varepsilon_A = \varepsilon_\infty + \frac{\varepsilon_L \gamma_L / 2}{(\omega_L - \omega) - i\gamma_L / 2}
$$

(S.22)

Here ε_L defines the strength of a Lorentzian and is equal to its contribution to the imaginary

part at the line center, $\varepsilon_A(\omega_L) = \varepsilon_\infty + i\varepsilon_L$, while γ_L is its FWHM. The gain material is

characterized by the non-dispersive Eqn. (S.10). Repeating the steps leading to (S.13), one

obtains:

$$\frac{\omega - \omega_L}{\gamma_L / 2} = \frac{\frac{1}{2}N\varepsilon_L - \sqrt{(\frac{1}{2}N\varepsilon_L)^2 - (N\varepsilon_\infty + \varepsilon_G')^2}}{N\varepsilon_\infty + \varepsilon_G'}, \quad -\varepsilon_G'' = \frac{1}{2}N\varepsilon_L - \sqrt{(\frac{1}{2}N\varepsilon_L)^2 - (N\varepsilon_\infty + \varepsilon_G')^2} \quad (S.23)$$

These are threshold expressions for an arbitrary shape factor N. For a Lorentzian absorber,

$\varepsilon_A' < 0$ only for $\omega > \omega_L$ and has a minimum there. As a result, each N produces two threshold

values with identical ε_A' values. The root closer to ω_L has much larger absorption and needs

much higher threshold gain. Hence, we give the formulas only for the second (strongly

detuned) root with the lower gain. The minimization of gain $-\varepsilon_G''$ with respect to N results in

the following values

$$
\begin{aligned}
N_{\min} &= \frac{\varepsilon_G'}{\varepsilon_\infty} \frac{\varepsilon_L^2 + 4\varepsilon_\infty^2}{\varepsilon_L^2 - 4\varepsilon_\infty^2} \overset{\varepsilon_L \gg \varepsilon_\infty}{\approx} \frac{\varepsilon_G'}{\varepsilon_\infty} \\
\frac{\omega_{\min} - \omega_L}{\gamma_L / 2} &= \frac{\varepsilon_L}{2\varepsilon_\infty} \overset{\varepsilon_L \gg \varepsilon_\infty}{\gg} 1, \quad -\varepsilon_{\min}'' = \frac{4\varepsilon_\infty \varepsilon_G' \varepsilon_L}{\varepsilon_L^2 - 4\varepsilon_\infty^2} \overset{\varepsilon_L \gg \varepsilon_\infty}{\approx} \frac{4\varepsilon_\infty \varepsilon_G'}{\varepsilon_L}
\end{aligned}
\quad (S.24)
$$

Here the last approximations refer to the most relevant case of a strong absorber $\varepsilon_L \gg \varepsilon_\infty$.

Condition $\varepsilon_L > 2\varepsilon_\infty$ is required in (S.22), so that $\varepsilon_A' < 0$ at least in some spectral range.

The last equalities in (S.24) show, that the thresholds can become low only for strong

absorbers. In this case the generation frequency lies on the far blue wing of the Lorentzian

line. In this region, $\varepsilon_A' < 0$ and both ε_A'' and $-\varepsilon_A'$ increase with increasing wavelength

(towards the center of the absorbing line). This leads to the competition between the

decreasing shape factor N and increasing absorption and the emergence of the optimal

condition in a similar way as discussed for the metals in the main text.

As an example, let us consider SiC, which has a very strong absorption line near $\lambda=12.6$ μm, with Lorentzian strength $\varepsilon_L \approx 248$ and background a value $\varepsilon_\infty \approx 6.7$ as adapted from [16, 18]. Assuming as before $\varepsilon_G' = 2.6$ for the active matrix, and using expressions (S.24) we obtain:

$$N_{min} = 0.39, \ \frac{\omega_{min} - \omega_L}{\gamma_L / 2} = 18.5, \ -\varepsilon_{min}'' = 0.28 \tag{S.25}$$

Thus, the generation with the lowest threshold takes place at a far blue slope of the Lorentzian line, exactly where Q-factors of the localized phonon-polariton resonances of nanostructures are high [16, 17]. The needed gain values become feasible for very strong absorbers, but are still about an order of magnitude higher than for the silver. This is because for metals $-\varepsilon_M'' / \varepsilon_M' \sim \gamma / \omega \ll 1$, while for Lorentzian absorbers $-\varepsilon_A'' / \varepsilon_A' \sim 1$ in the center of the line, and $-\varepsilon_A'' / \varepsilon_A' \sim \gamma_L / (\omega - \omega_L) \ll 1$ on its wings. In other words, metals are "better oscillators" from the point of view of active plasmonics.

Supp. Info. 6. Quasi-static core-shell multipoles

Here we consider quasi-static multipolar denominators of spherical core-shell structures. Our geometry is shown in the inset in Fig. 3, namely a core with a radius a_1 and dielectric constant ε_1, a shell with a radius a_2 and dielectric constant ε_2, immersed in the ambient medium with a dielectric constant ε_3. The shell thickness $h_2 = a_2 - a_1$. The lowest (zero order) term in the Taylor expansion of the full multi-shell Mie multipolar denominator from [19] with respect to vacuum wavenumber k is:

$$D_l \sim [l\varepsilon_1 + (l+1)\varepsilon_2][l\varepsilon_2 + (l+1)\varepsilon_3] + l(l+1)\left(\frac{a_1}{a_2}\right)^{2l+1}(\varepsilon_1 - \varepsilon_2)(\varepsilon_2 - \varepsilon_3) \tag{S.26}$$

Higher order terms yield retardation corrections, as for the spheres in Supp. Info. 2, but for brevity we restrict ourselves to the quasi-static term. Similar formulas in the literature often contain inaccuracies. For example in Ref. [20], Eqn. (7.12), has a factor $(a_1 / a_2)^3$ instead of

$(a_1 / a_2)^{2l+1}$ in the quasi-static multipolar term; in Ref. [1], Eqn. (5.36) and Ref. [3], Eqn. (2.33a), consider the dipolar case only, and the latter contains a factor $(2\varepsilon_2 - \varepsilon_3)$ instead of $2(\varepsilon_2 - \varepsilon_3)$; in Ref. [21], Eqn. (1), gives the correct expression for the multipolar resonant frequency, but only for a non-absorbing Drude shell in vacuum.

In the symmetric two-materials case with $\varepsilon_3 = \varepsilon_1$ Eqn. (S.26) becomes quadratic in ε_1 and ε_2, and can be rewritten as:

$$D_l \sim (\varepsilon_1 + N_+\varepsilon_2)(\varepsilon_1 + N_-\varepsilon_2) \tag{S.27}$$

Here we introduced the notations:

$$N_\pm = g - 1 \pm \sqrt{g(g-2)}, \;\; g = \frac{(2l+1)^2}{2l(l+1)(1-(a_1/a_2)^{2l+1})} \tag{S.28}$$

As the threshold corresponds to zero of denominator (S.27), $D_l = 0$, the parameters $N_\pm$ are examples of the general multipolar shape parameter N from the Eqn. (5) in the main text. They are valid for *arbitrary quasi-static symmetric* core-shell with $\varepsilon_1 = \varepsilon_3 = \varepsilon_G$. To obtain compact illustrative formulas for *thin* shells $h_2 \ll a_1$, one can make further simplifications using the approximation:

$$\left(\frac{a_1}{a_2}\right)^{2l+1} = \left(\frac{a_1}{a_1+h_2}\right)^{2l+1} \overset{h_2 \ll a_1}{\approx} 1 - (2l+1)\frac{h_2}{a_1} \tag{S.29}$$

In this case, the multipolar shape parameters $N_\pm$ in Eqns. (S.27)-(S.28) up to the leading order in h_2 / a_1 become:

$$N_+ \approx \frac{2l+1}{l(l+1)}\frac{a_1}{h_2}, \;\; N_- \approx \frac{l(l+1)}{2l+1}\frac{h_2}{a_1} \tag{S.30}$$

The first of these expressions is large, and the second is small; for $\varepsilon_1 = \varepsilon_G$, $\varepsilon_2 = \varepsilon_M$ the latter leads to the expression (9) in the main text.

It is worth mentioning, that a thin active shell $\varepsilon_2 = \varepsilon_G$ in a symmetric metallic environment $\varepsilon_1 = \varepsilon_3 = \varepsilon_M$ results in exactly the same condition for the ε_2 of the gain medium:

$$\varepsilon_2 = -\frac{l(l+1)}{(2l+1)}\frac{h_2}{a_1}\varepsilon_1, \quad \varepsilon_2 = -\frac{(2l+1)}{l(l+1)}\frac{a_1}{h_2}\varepsilon_1 \qquad (S.31)$$

Similar formulas for the asymmetric case $\varepsilon_1 \neq \varepsilon_3$ can be obtained from Eqn. (S.26), which is

linear in ε_1 or ε_3. For example, assuming that the gain material is in the core only (the

situation discussed in [15] and studied in detail for $l = 1$ in Ref. [22]), we can write:

$$\varepsilon_1 = -L\frac{(1-f)\varepsilon_2 + (L+f)\varepsilon_3}{(1+Lf)\varepsilon_2 + L(1-f)\varepsilon_3}\varepsilon_2, \qquad L = \frac{l+1}{l}, \qquad f = \left(\frac{a_1}{a_2}\right)^{2l+1} \qquad (S.32)$$

In thin shell approximation, this results in:

$$\varepsilon_1 \overset{h_2 \ll a_1}{\approx} -\frac{l+1}{l}\left[\varepsilon_3 + (l\varepsilon_2 + (l+1)\varepsilon_3)\frac{\varepsilon_2 - \varepsilon_3}{\varepsilon_2}\frac{h_2}{a_1}\right] \qquad (S.33)$$

For vanishing shell $h_2 \to 0$ one recovers the equations (7) and (8) for the sphere 1 in the

ambient material 3. If the ambient material is transparent, $.\varepsilon_3'' = 0.$, one can easily separate the

real and imaginary parts here. In the lowest orders in h_2/a_1 this results in:

$$\varepsilon_1' \approx -\frac{l+1}{l}\varepsilon_3, \quad \varepsilon_1'' \approx -(l+1)(1+\frac{l+1}{l}\frac{\varepsilon_3^2}{|\varepsilon_2|^2})\varepsilon_2''\frac{h_2}{a_1} \qquad (S.34)$$

The imaginary part of the gain material ε_1 becomes small for thin shells with $h_2 \ll a_1$, and

we can expect low thresholds for the asymmetric core-shell, similarly to the situation

described by the expression (9). However, the resonant wavelength is largely determined by

the first term in the r.h.s. of the Eqn. (S.33), which implies that quasi-static "material

resonances" might be absent altogether for the very thin core-shell in asymmetric background.

For the asymmetric case of metallic core with gain shell in neutral background, used in

experiments [23], equating $D_l = 0$ in (S.26), and resolving the quadratic equation with respect

to ε_2, one obtains 2 roots (with notations from (S.32)):

$$\varepsilon_2 = -b \pm \sqrt{b^2 - \varepsilon_1\varepsilon_3}, \quad b = \frac{(Lf+1)\varepsilon_1 + L(L+f)\varepsilon_3}{2L(1-f)} \qquad (S.35)$$

When the gain shell is thick with respect to the core radius $(f \rightarrow 0)$, one recovers the

resonances for the inner and outer spheres:

$$\varepsilon_2 = -\frac{l}{l+1}\varepsilon_1, \quad \varepsilon_2 = -\frac{l+1}{l}\varepsilon_3 \qquad (S.36)$$

From the structure of solutions (S.35) one infers, that the resonances are close to these
limiting values if:

$$Lf \ll 1, \qquad \overset{\text{for } l=1, L=2}{\Rightarrow} \qquad \frac{h_2}{a_1} \gg 2^{1/3} - 1 \approx 0.26 \qquad (S.37)$$

This is not a very stringent requirement, with $h_2 / a_1 \approx 2.14$ in Ref. [23], though their structure

included a spacer and assumed inhomogeneous gain layer, which results in 5-materials system.

The threshold there is within ~10% from the one obtained using Eq. (S.35), the latter being

~5% higher than the 1st estimate in (S.36). This confirms that 2-materials case usually

provides a lower limit for the threshold in more complex multiple-materials structures.

We emphasize, that only the exact full, multi-shell Mie formulas with retardation were used in

the Section 5 of the main text.

Supp. Info. 7. Threshold for the near-field plasmon between 2 spheroids

In many experimental and theoretical studies, pairs or several MNPs are used to tune or to

strengthen plasmonic resonances [24, 25]. For the "bright, in phase" dipolar mode of metallic

dimers, the field enhancement in the gap between the particles increases significantly, and the

mode volume decreases. One might expect that this may decrease the spasing threshold if the

gap is filled with a gain material. Here we illustrate that this is not the case, using simple

example of identical spheroidal dipoles, aligned in *z*-direction along their common axis. The

consideration is similar for other geometries. Due to interaction between such "dimer nano-

antennas", the system can be characterized by the effective polarizability, see *e.g.*, [26], which

self-consistently includes the action of dipoles onto each other. Effective polarizability

includes the resonant denominator, accounting for double-scattering round trip of light

between the particles. In the near field, when both dipoles are separated by the distance R and point in the same z-direction from one to another (which is the most favorable case for threshold minimization), the denominator of the effective polarizability is $D_{12} = 1 - 4\alpha^2 R^{-6}$.

Here $\alpha = \dfrac{V(\varepsilon_M - \varepsilon_G)}{4\pi(\varepsilon_M L + \varepsilon_G(1-L))}$ is the polarizability of the individual spheroid, and the $4R^{-6}$

term comes from the near field dipole interaction in both directions. This is similar to Förster resonance energy transfer (FRET).

The generation threshold in such a 2-particle system corresponds to a singularity in the *effective* polarizability, i.e., to a condition $D_{12} = 0$. This implies:

$$D_{12} = 1 - 4\alpha^2 R^{-6} = 0 \Rightarrow \alpha = \frac{V(\varepsilon_M - \varepsilon_G)}{4\pi(\varepsilon_M L + \varepsilon_G(1-L))} = \frac{R^3}{2} \Rightarrow$$

$$\varepsilon_M L + \varepsilon_G(1-L) = \frac{2a^2 c}{3R^3}(\varepsilon_M - \varepsilon_G) \Rightarrow \varepsilon_M(L-v) + \varepsilon_G(1-L+v) = 0$$

(S.38)

Here we introduced additional geometrical factor $v = \dfrac{2a^2 c}{3R^3}$, related to the inter-particle

distance R and spheroid semi-axes c (axis of revolution) and a (notations are as in Supp. Info. 1). The last resonant condition has exactly the same form as the general expression (5) for the individual particle.

$$\varepsilon_G = -\underbrace{\frac{L-v}{1-L+v}}_{N_{pair}}\varepsilon_M$$

(S.39)

The only difference is, that the shape factor N_{pair}, besides the depolarization factor L, now contains the additional parameter v related to the volume and distance. This shifts the resonance, and for a given individual particle shape (characterized by L) makes $N_{pair} < N$ for a single spheroid. However, as the functional relation (5) between ε_G and ε_M stays intact, the conditions (11) and the global optimum remain the same. Naturally, it occurs for a different geometry of an *individual* particle, as can be recalculated from (S.39), which can also be

useful for a qualitative understanding of resonances in metallic dimers without gain. The

position of such "cold" (gain-less) resonances is determined by the real part of (S.39). For a

constant ε_G' and a typical metal, a decrease in N_{pair} shifts the resonance towards larger $-\varepsilon_M'$,

that is to larger wavelengths. This means, that an increase in volume $V \propto a^2 c$, or a decrease in

inter-particle distance R, increase v and lead to a red shift of the "in-phase", "bright" mode

considered here even for small non-retarded Rayleigh particles. A similar approach can be

applied to other modes. For realistic particle sizes, one usually has to consider retardation to

obtain quantitative results.

This argumentation remains valid for arbitrary near-field geometries. For far-field systems

like conventional or random lasers, this does not hold. In such structures, arbitrarily low

thresholds can be realized, utilizing amplification harvested from the large volumes of gain

material, competing with the relatively small Ohmic losses on metallic mirrors or scatterers.

Supp. Info. 8. Equivalence to the threshold formulation via complex eigenvalue

Sometimes the generation threshold is defined as disappearance of the imaginary part of a

complex eigenfrequency ω for the spasing mode [23]. This definition of threshold is

equivalent to the condition $D_l=0$ in (14), which is used here and in other works [27, 28]. This

can be explained as follows.

With the incident field, the scattering problem is an inhomogeneous boundary-value problem.

Boundary conditions at the outer boundary of the structure result in a system of

inhomogeneous linear equations for the fields on both sides of the boundary (for example for

E and **H**, more accurately for the coefficients in the corresponding eigenfunction expansion).

Its solution is the ratio of two determinants. The numerator includes the column of "free

terms" made of incident fields, while the denominator is made of the coefficient matrix of the

homogeneous system. The complex equality $D_l(\varepsilon_G'', \omega, ...) = 0$ allows one to find two real

numbers: the threshold gain ε_{thr}'' and the generation frequency ω_{thr}.

The eigenmodes of the spasing structure are the solutions of the same boundary-value

problem, but without the external field. The corresponding boundary conditions yield a

system of *homogeneous* linear equations with the same coefficient matrix as for the scattering

problem. This system is consistent and has solutions only when its complex determinant

equals zero, $D_l(\varepsilon_G'', \omega, ...) = 0$. This yields a set of complex eigenfrequencies

$\omega = \omega'(\varepsilon_G'', ...) + i\omega''(\varepsilon_G'', ...)$. Without gain ($\varepsilon_G'' = 0$), or for small gain, for the $e^{-i\omega t}$ sign

convention, $\omega'' < 0$ describes the energy decay, but for a big enough (negative) gain

$\varepsilon_G'' = \varepsilon_{thr}'' < 0$ the decay disappears $\omega''(\varepsilon_{thr}'', ...) = 0$, which corresponds to the generation

threshold. The real part of the eigenvalue at this gain yields the generation (spasing)

frequency $\omega_{thr} = \omega'(\varepsilon_{thr}'', ...)$.

Thus, in both cases, the threshold parameters ω_{thr} and ε_{thr}'' are found from the condition

$D_l(\varepsilon_{thr}'', \omega_{thr}, ...) = 0 + i0$, which proves the equivalence of both approaches. Far from the

threshold the interrelation between the two approaches is less straightforward.

References Supporting Information

[1]   C. F. Bohren and D. R. Huffman, *Absorption and scattering of light by small particles*.

       (Wiley, New York, 1998).

[2]   M. Born and E. Wolf, *Principles of optics : electromagnetic theory of propagation,*

       interference and diffraction of light, 7th expanded ed. (Cambridge University Press,

       Cambridge ; New York, 1999).

[3]   U. Kreibig and M. Vollmer, *Optical properties of metal clusters*. (Springer, Berlin ;

       New York, 1995).

[4]   J. D. Jackson, *Classical electrodynamics*, 3rd ed. (Wiley, New York, 1999).

[5]   M. Meier and A. Wokaun, Opt. Lett. **8** (11), 581-583 (1983).

[6]   D. Schebarchov, B. Auguie and E. C. Le Ru, Physical Chemistry Chemical Physics **15** (12), 4233-4242 (2013).

[7]   A. Moroz, J Opt Soc Am B **26** (3), 517-527 (2009).

[8]   S. A. Maier, *Plasmonics : fundamentals and applications*. (Springer, New York, 2007).

[9]   G. C. des Francs, Int J Mol Sci **10** (9), 3931-3936 (2009).

[10]   A. Alu and A. Salandrino, Opt Express **14** (4), 1557-1567 (2006).

[11]   V. P. Drachev, U. K. Chettiar, A. V. Kildishev, H. K. Yuan, W. S. Cai and V. M. Shalaev, Opt Express **16** (2), 1186-1195 (2008).

[12]   X. Ni, Z. Liu, F. Gu, M. G. Pacheco, J. Borneman and A. V. Kildishev, (2012), pp. https://nanohub.org/resources/6977.

[13]   N. V. Karlov, *Lectures on quantum electronics*. (Mir Publishers; CRC Press, Moscow; Boca Raton, Fla., 1993).

[14]   A. E. Siegman, *Lasers*. (University Science Books, Mill Valley, Calif., 1986).

[15]   M. I. Stockman, Journal of Optics **12** (2), 024004 (2010).

[16]   T. Wang, P. N. Li, B. Hauer, D. N. Chigrin and T. Taubner, Nano Letters **13** (11), 5051-5055 (2013).

[17] J. D. Caldwell, O. J. Glembocki, Y. Francescato, N. Sharac, V. Giannini, F. J. Bezares, J. P. Long, J. C. Owrutsky, I. Vurgaftman, J. G. Tischler, V. D. Wheeler, N. D. Bassim, L. M. Shirey, R. Kasica and S. A. Maier, Nano Letters **13** (8), 3690-3697 (2013).

[18]   E. D. Palik and G. Ghosh, *Handbook of optical constants of solids*. (Academic Press, San Diego, 1997).

[19]   G. Raschke, PhD, Ludwig–Maximilians–Universität, 2005.

[20]   M. Quinten, *Optical properties of nanoparticle systems: Mie and beyond*. (Wiley-VCH, Weinheim, Germany, 2011).

[21] E. Prodan, C. Radloff, N. J. Halas and P. Nordlander, Science **302** (5644), 419-422 (2003).

[22] D. G. Baranov, E. S. Andrianov, A. P. Vinogradov and A. A. Lisyansky, Opt Express **21** (9), 10779-10791 (2013).

[23] M. A. Noginov, G. Zhu, A. M. Belgrave, R. Bakker, V. M. Shalaev, E. E. Narimanov, S. Stout, E. Herz, T. Suteewong and U. Wiesner, Nature **460** (7259), 1110-U1168 (2009).

[24] T. Hanke, J. Cesar, V. Knittel, A. Trugler, U. Hohenester, A. Leitenstorfer and R. Bratschitsch, Nano Letters **12** (2), 992-996 (2012).

[25] J. Aizpurua, G. W. Bryant, L. J. Richter, F. J. G. de Abajo, B. K. Kelley and T. Mallouk, Phys Rev B **71** (23), 235420 (2005).

[26] S. Toroghi and P. G. Kik, Appl Phys Lett **100** (18), 183105 (2012).

[27] N. Arnold, B. Y. Ding, C. Hrelescu and T. A. Klar, Beilstein J Nanotech **4**, 974-987 (2013).

[28] X. G. Meng, U. Guler, A. V. Kildishev, K. Fujita, K. Tanaka and V. M. Shalaev, Sci Rep **3**, 1241 (2013).